An asymmetric SMC–kleisin bridge in prokaryotic condensin

Frank Bürmann[1,5], Ho-Chul Shin[2,5], Jérôme Basquin[3,5], Young-Min Soh[2], Victor Giménez-Oya[1], Yeon-Gil Kim[4], Byung-Ha Oh[2] & Stephan Gruber[1]

Eukaryotic structural maintenance of chromosomes (SMC)–kleisin complexes form large, ring-shaped assemblies that promote accurate chromosome segregation. Their asymmetric structural core comprises SMC heterodimers that associate with both ends of a kleisin subunit. However, prokaryotic condensin Smc–ScpAB is composed of symmetric Smc homodimers associated with the kleisin ScpA in a postulated symmetrical manner. Here, we demonstrate that Smc molecules have two distinct binding sites for ScpA. The N terminus of ScpA binds the Smc coiled coil, whereas the C terminus binds the Smc ATPase domain. We show that in *Bacillus subtilis* cells, an Smc dimer is bridged by a single ScpAB to generate asymmetric tripartite rings analogous to eukaryotic SMC complexes. We define a molecular mechanism that ensures asymmetric assembly, and we conclude that the basic architecture of SMC–kleisin rings evolved before the emergence of eukaryotes.

Members of the SMC and kleisin ('closure') families of proteins are conserved in all domains of life and have key roles in the maintenance of chromosomes[1,2]. In eukaryotes, several SMC–kleisin complexes operate during and after DNA replication to promote chromosome segregation in mitosis and meiosis. Cohesin mediates sister-chromatid cohesion, promotes DNA double-strand-break repair and regulates gene expression[2]. Condensin is pivotal for the reshaping of chromosomes during prophase and ensures timely and efficient separation of sister chromatids during anaphase[1,3,4]. A third SMC complex, comprising Smc5 and Smc6, is involved in DNA repair and was recently implicated in relieving replication-induced topological stress[5,6].

Condensin complexes in prokaryotes are usually of the Smc–ScpAB type and are formed by the canonical SMC and kleisin proteins Smc and ScpA, respectively, and the third subunit ScpB[7–10]. However, some bacterial species, including *Escherichia coli*, have condensin (MukBEF) formed by deviant homologs MukB, MukE and MukF[11,12]. Condensin mutations are lethal in *B. subtilis* and *E. coli* under conditions promoting fast growth[9,11]. On minimal media or at low temperature, however, the mutants are viable but produce anucleate progeny at a high frequency, which is indicative of severe chromosome segregation defects. In *B. subtilis* and *Streptococcus pneumoniae*, Smc–ScpAB is recruited to the origin of replication (*oriC*) region by ParB proteins bound to *parS* sites[13–15]. How MukBEF is targeted to the origin region in *E. coli* is unknown[16].

SMC proteins share a unique architecture comprising two globular domains—a nucleotide-binding domain (NBD) of the ABC-type ATPase fold (SMC head) and a central hinge domain—connected by a long antiparallel intramolecular coiled coil (**Fig. 1a**). The hinge domain mediates dimerization of SMC proteins, producing V-shaped SMC homodimers in prokaryotes and heterodimers in eukaryotes[17–19]. Proper function of SMC proteins and their normal association with chromosomes requires the NBDs of SMC proteins to undergo a cycle of ATP binding, nucleotide-dependent engagement with a second NBD and engagement-dependent hydrolysis of ATP[20–24].

SMC protein dimers associate with additional subunits, one of which generally belongs to the kleisin family of proteins[25]. Kleisins contain a winged-helix domain at their C terminus (cWHD) that interacts with the bottom surface (termed 'cap' region) of SMC heads. In the case of cohesin, the cWHD of kleisin Scc1 binds the NBD of Smc1 but not Smc3 (refs. 20,26). Instead, Smc3 is specifically bound by the N terminus of Scc1 ($Scc1^N$) through a poorly defined interface[26]. Smc1 and Smc3 proteins held together at the hinge are additionally bridged by kleisin, thereby creating stable tripartite rings that associate with and entrap chromosomes[26–28].

The best-characterized bacterial SMC–kleisin assembly is MukBEF of *E. coli*. Because dimers formed by its SMC subunit MukB are homotypic, each MukB dimer contains two NBDs that can interact with cWHDs of the kleisin MukF[29]. Concomitantly, the N-terminal region of MukF folds into a helical bundle and another WHD, which together mediate stable dimerization of MukF[29,30]. Thus, MukF dimers interact with dimeric MukB to form either symmetric tetrapartite rings or larger oligomeric assemblies[29,31]. Clearly, the overall architecture of cohesin and MukBEF is very different. It is not clear whether the MukBEF architecture is a unique feature of this evolutionarily deviant complex or a general attribute of complexes comprising symmetric

[1]Max Planck Research Group Chromosome Organization and Dynamics, Max Planck Institute of Biochemistry, Martinsried, Germany. [2]KAIST Institute for the Biocentury, Department of Biological Sciences, Korea Advanced Institute of Science and Technology, Daejeon, Korea. [3]Department of Structural Cell Biology, Max Planck Institute of Biochemistry, Martinsried, Germany. [4]Pohang Accelerator Laboratory, Pohang University of Science and Technology, Pohang, Korea. [5]These authors contributed equally to this work. Correspondence should be addressed to B.-H.O. (bhoh@kaist.ac.kr) or S.G. (sgruber@biochem.mpg.de).

Received 20 September 2012; accepted 7 December 2012; published online 27 January 2013; doi:10.1038/nsmb.2488

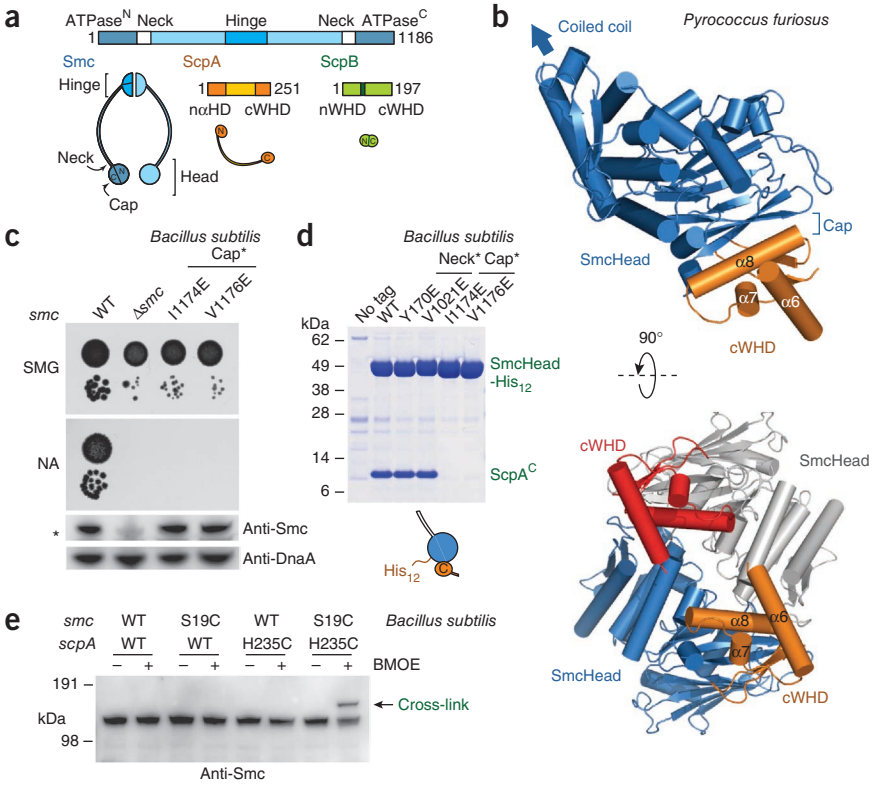

Figure 1 ScpA's winged-helix domain associates with Smc. (**a**) Domain organization of Smc, ScpA and ScpB proteins. Residue numbering corresponds to *B. subtilis* proteins. (**b**) Crystal structure of the SmcHead–ScpA^C complex from *P. furiosus*. Side view of a Smc head associated with SpcA's cWHD (top). Bottom view of the asymmetric unit comprising a dimeric complex of SmcHead–ScpA^C (bottom). ScpA and Smc features are shown in orange or red and blue or gray, respectively. (**c**) Colony formation by mutant *B. subtilis* strains. Diluted cultures of BSG2, BSG68, BSG732 and BSG731 are shown spotted on minimal medium agar (SMG) or nutrient agar (NA), with expression levels of mutant Smc proteins determined by immunoblotting using Smc- and DnaA-specific antisera. A cross-reacting band migrating slightly faster than Smc is marked by asterisk. WT, wild type. (**d**) Pulldown assays using recombinant ScpA^C and SmcHead. SDS-PAGE and Coomassie staining of eluate fractions from histidine-tag purification of wild-type and mutant SmcHead-His$_{12}$ from *B. subtilis*, co-expressed with ScpA^C in *E. coli*, are shown. (**e**) Cysteine cross-linking of Smc and ScpA proteins in *B. subtilis*. Immunoblotting using Smc-specific antiserum is shown. Samples are from strains BSG2, BSG360, BSG367 and BSG372, grown in LB medium and incubated on ice with BMOE (+) or dimethyl sulfoxide (DMSO) alone (–).

SMC dimers. There is limited sequence similarity between the N-terminal part of ScpA and eukaryotic kleisins and between ScpA and MukF[25,30], which indicates that ScpA might function either as a monomer like Scc1 or as a dimer like MukF. The current widely accepted notion is that Smc–ScpAB complexes are closely related to the symmetric MukBEF complex[1,3]. Recently, however, purified ScpA has been shown to be monomeric in solution[32], thus potentially challenging this assumption.

Here, we set out to determine the molecular architecture of Smc–ScpAB *in vitro* and *in vivo*.

RESULTS

The winged-helix domain of ScpA binds Smc

Kleisin's cWHD associates with the SMC cap region in MukBEF and cohesin[20,29]. To investigate whether this interaction is conserved in Smc–ScpAB, we determined the structure of a complex between the head domain of Smc (SmcHead) and the C terminus of ScpA (residues 126–212; ScpA^C) derived from *Pyrococcus furiosus* to 2.3-Å resolution (**Table 1**). The asymmetric unit of the crystal contained two copies of SmcHead–ScpA^C, which interact with each other similarly to two head domains that are engaged by binding to ATP[20,21]. ScpA^C is composed of a WHD that is bound to the cap region of SmcHead (**Fig. 1b** and **Supplementary Fig. 1a**), as previously observed for cohesin and MukBEF[20,29].

To investigate the physiological relevance of this interaction, we designed single–amino acid substitution mutants of (bacterial) Smc that prevent interaction with cWHD. Hydrophilic substitution of Ile1174 and Val1176 in *B. subtilis* Smc, which correspond to Val1153 and Leu1155 in the *P. furiosus* structure, respectively, were predicted to disrupt the binding interface. Smc^{I1174E} and Smc^{V1176E} strains failed to grow on rich medium (nutrient agar) and formed colonies more slowly than did wild type on minimal medium, similarly to a deletion mutant of *smc* (**Fig. 1c**). Pulldown assays with recombinantly coexpressed *B. subtilis* (Bs) SmcHead-His$_{12}$ and ScpA^C showed that both cap mutations abolish interaction with ScpA^C (**Fig. 1d**). Finally, we directly tested whether this interaction occurs in *B. subtilis* cells with Smc–ScpAB complexes in their endogenous context. On the basis of the gained structural information (**Fig. 1b**), we introduced—by allelic replacement—pairs of cysteine residues into Smc and ScpA that can be cross-linked by the thiol-specific compound bismaleimidoethane (BMOE) (**Supplementary Fig. 1b**). Cells were grown to exponential phase, then incubated on ice with BMOE and analyzed by immunoblotting. Smc^{S19C} produced an additional band after cross-linking only in the presence of ScpA^{H235C} (**Fig. 1e**). Together, these findings establish that interaction of cWHD with the cap region of Smc is evolutionarily conserved and crucial for the functionality of Smc–ScpAB in *B. subtilis*.

Structure of ScpAB forming an asymmetric 1:2 complex

Next, we investigated the structural role of ScpB and the N-terminal domain of ScpA for the formation of Smc–ScpAB complexes. N-terminal sequences in the *E. coli* kleisin MukF fold into a WHD and a four-helix bundle that drive stable dimerization of two MukF–MukE$_2$ subcomplexes (MukEF)[29,30]. ScpA conceivably forms similar dimeric structures[33]. We determined the structure of a truncated *S. pneumoniae* ScpA lacking its cWHD (ScpA$^{\Delta C}$; **Fig. 2a**) bound to ScpB with a C-terminal truncation of six residues (ScpB) to a resolution of 2.8 Å (**Table 1**). ScpA$^{\Delta C}$ is seen to form a complex with two molecules of ScpB (ScpB$_A$ and ScpB$_B$; **Fig. 2b**). As previously observed[34], both ScpB proteins comprise two WHDs. However, in this structure they form an asymmetric head-to-head dimer through interaction of their nWHDs (**Fig. 2b** and **Supplementary Fig. 2a**). ScpA$^{\Delta C}$ is composed of two domains: an N-terminal α-helical domain with three α-helices (nαHD) and a central domain that can be subdivided into a central ~49-Å-long α-helix (α4), a long loop and a terminal α-helix (α5) (**Fig. 2b**). Overall, ScpA bound to ScpB$_A$ and ScpB$_B$ at its central domain forms a rope-like structure with two globular domains at the N and C termini.

Table 1 Data collection and refinement statistics

	PfSmcHead–ScpA^{C}	SpScpA$^{\Delta C}$–ScpB	BsSmcHead–ScpA^{N}
Data collection			
Space group	$P4_1$	$C2$	$P4_3$
Cell dimensions			
a, *b*, *c* (Å)	117.86, 117.86, 94.48	185.3, 82.72, 59.91	107.43, 107.43, 102.82
α, β, γ (°)	90, 90, 90	90, 98.9, 90	90, 90, 90
	Peak	*Peak*	*Peak*
Wavelength	0.9793	0.9793	0.9793
Resolution (Å)[a]	30.00–2.30 (2.34–2.30)	50.00–2.80 (2.85–2.8)	75.97–3.40 (3.58–3.4)
R_{sym}	9.0 (32.6)	8.5 (90.7)	8.7 (58.8)
$I / \sigma I$	31.8 (4.3)	39.6 (3.0)	18.8 (3.3)
Completeness (%)	99.9 (99.8)	99.9 (99.8)	99.9 (99.2)
Redundancy	10.4 (7.8)	7.4 (7.5)	9.5 (9.1)
Refinement			
Resolution (Å)	30.00–2.30	50.00–2.80	75.97–3.40
No. reflections	51,756	22,073	16,149
R_{work} / R_{free}	21.5 / 22.9	23.9 / 25.9	25.45 / 27.2
No. atoms			
Protein	6,132	3,768	6,339
Ligand/ion	15	0	0
Water	91	4	0
B factors			
Protein	44.423	93.407	109.42
Ligand	34.550	–	–
Water	34.978	37.100	–
r.m.s. deviations			
Bond lengths (Å)	0.007	0.008	0.01
Bond angles (°)	1.3	1.3	1.5

[a]One crystal was used for each structure.

The asymmetric 1:2 complex between ScpA$^{\Delta C}$ and ScpB does not exhibit tight interactions with neighboring symmetry-related molecules, which indicates that ScpA and ScpB of *S. pneumoniae*, unlike MukE and MukF, form a 1:2 complex as the biological unit. This is consistent with a recent atomic force microscopic study indicating that ScpA and ScpB of *B. subtilis*, a closely related species, might form a ScpA–ScpB$_2$ complex (ScpAB)[32].

Essential interaction between ScpA and the Smc coiled coil

The overall structures of ScpAB and MukEF are substantially different (**Supplementary Fig. 2b**,**c**), which raises the question of what role ScpA's nαHD might have in Smc–ScpAB assembly. In cohesin, Scc1^{N} interacts with Smc3 through a poorly defined interface[26]. To test whether the N-terminal domain of ScpA binds Smc, we coexpressed a fragment of *B. subtilis* ScpA (residues 1–86; ScpA^{N}) together with full-length Smc protein in *E. coli*. Smc was efficiently co-purified with ScpA^{N}-His$_6$, and the two proteins formed a stable complex that eluted in size-exclusion chromatography as a single peak (**Fig. 3a**).

SmcHead (including a stretch of coiled coil called the 'neck' region) also formed a tight protein complex with ScpA^{N}-His$_6$ (**Fig. 3a** and **Supplementary Fig. 3a**). Similarly, an Smc neck fragment associated with ScpA^{N}-His$_6$ (**Fig. 3a**). Together, these results imply that a stretch of coiled coil directly adjacent to the Smc NBD contains the binding site for ScpA^{N}. To test whether the neck region is important for Smc function *in vivo*, we mutated conserved residues in the Smc neck. Mutations Y170E and V1021E rendered Smc nonfunctional (**Fig. 3b**) and severely affected the interaction of SmcHead-His$_{12}$ with ScpA^{N} *in vitro* (**Fig. 3c**), whereas they did not interfere with binding to ScpA^{C} (**Fig. 1d**). The interaction between Smc and ScpA^{N} thus appears to be essential in *B. subtilis*.

To measure binding of ScpA^{N} to Smc *in vivo*, we modified this interface with cysteine residues that can be cross-linked by BMOE as described above. Because of the lack of structural information, we performed a systematic cysteine-scanning screen of poorly conserved residues in the interacting regions. The Smc^{R1032C} protein displayed specific cross-linking to either ScpA^{V50C} or ScpA^{E52C} (**Fig. 3d** and **Supplementary Table 1**), which suggests that these residues are closely juxtaposed in Smc–ScpAB *in vivo*.

A three-stranded coiled coil formed by the Smc neck and ScpA^{N}

We then determined the structure of the nucleotide-free SmcHead–ScpA^{N} complex derived from *B. subtilis* to 3.4-Å resolution (**Table 1**). In this structure, ScpA^{N} is composed of two α-helical stretches connected by a short loop (**Fig. 3e**). The longer C-terminal helix of ScpA^{N} comprises helices α2 and α3 observed in the ScpA$^{\Delta C}$–ScpB

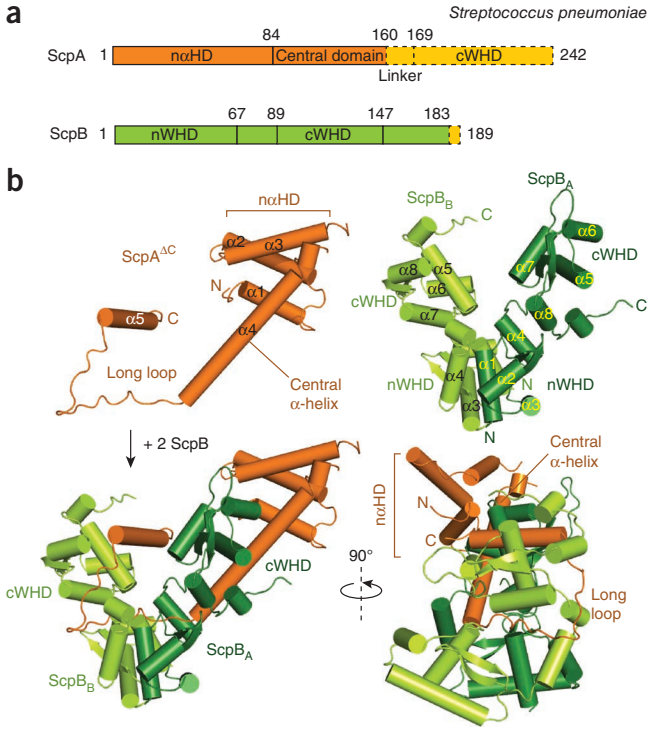

Figure 2 Organization of ScpAB. (**a**) Scheme depicting the domains of ScpA and ScpB. Numbers correspond to amino acid sequences of *S. pneumoniae*. Truncations introduced for structure determination are shown with dashed lines. (**b**) Crystal structure of the ScpA$^{\Delta C}$ monomer and the ScpB dimer from *S. pneumoniae* (top left and right, respectively). Structure of the ScpA$^{\Delta C}$–ScpB complex in two side views (bottom). ScpA and ScpB features are shown in orange and green, respectively.

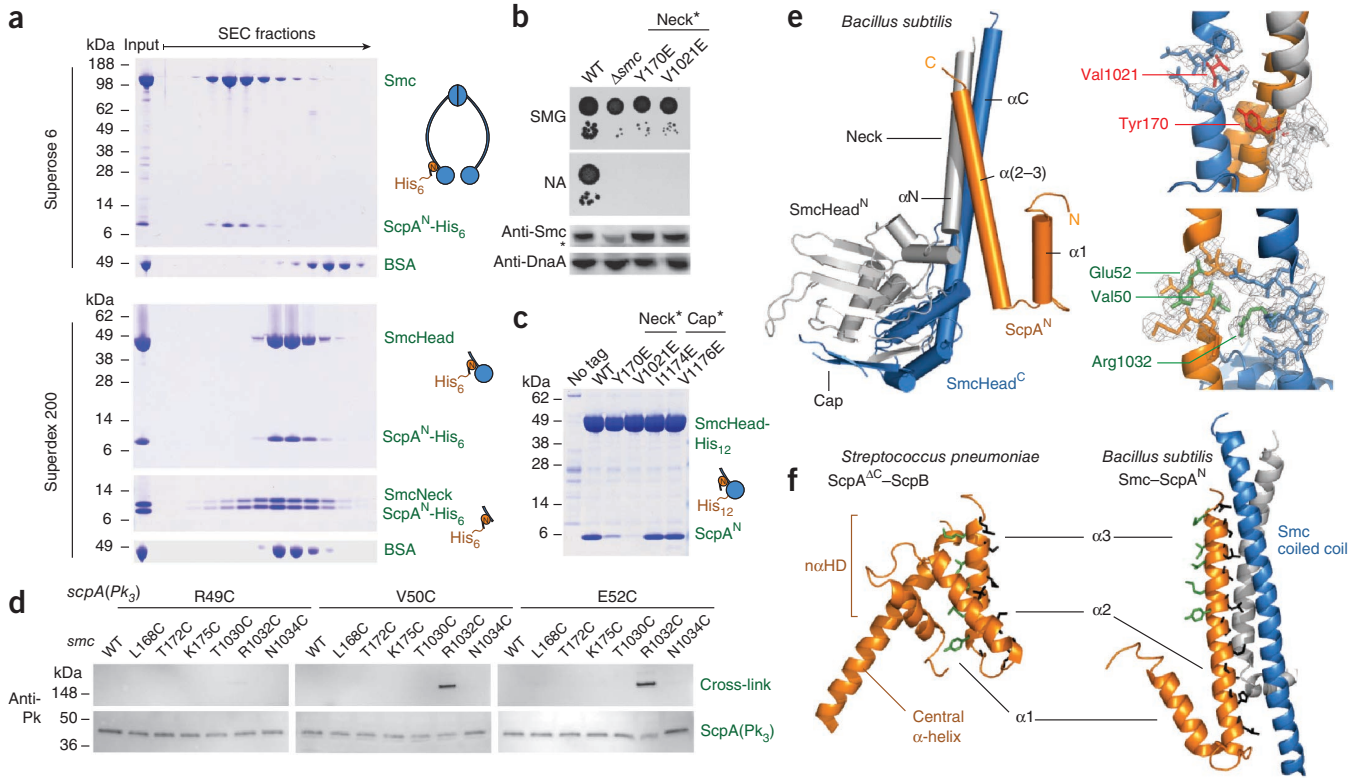

Figure 3 Structure of a second SMC–kleisin interface. (**a**) SDS-PAGE and Coomassie-staining analysis of proteins eluted from size-exclusion chromatography (SEC) columns. Samples are *B. subtilis* Smc and fragments thereof, coexpressed with ScpA^{N}-His$_6$ in *E. coli*, purified by using the histidine tag and fractionated by gel filtration. Bovine serum albumin (BSA) was fractionated as a size marker. (**b**) Colony formation by neck-mutant *smc* strains. Strains BSG2, BSG68, BSG508 and BSG511 examined for growth and Smc protein levels as in **Figure 1c** are shown. (**c**) Pulldown assay using recombinant ScpA^{N} and SmcHead-His$_{12}$. As in **Figure 1d**, using ScpA^{N} instead of ScpA^{C}. (**d**) A screen for juxtaposed residues at the Smc–ScpA^{N} interface. *B. subtilis* cells with engineered cysteine codons in *smc* and *scpA*(*Pk*$_3$) were screened for BMOE cross-linking by immunoblotting using anti-Pk antibodies. Full immunoblots are shown in **Supplementary Figure 3f**. (**e**) Structure of the SmcHead–ScpA^{N} complex from *B. subtilis*. Side view of the Smc head domain and ScpA^{N} (left). ScpA and N- and C-terminal Smc features are shown in orange, gray and blue, respectively. $2F_o$–F_c electron-density maps of selected residues at 3.4-Å resolution and contoured at 1σ are shown (right). Residues mutated to glutamate are indicated in red (top). Side chains mutated to cysteine are shown in green (bottom). (**f**) Structural transition in ScpA's nαHD upon binding to Smc. Helices α2 and α3 from nαHD in *S. pneumoniae* ScpA^{ΔC}–ScpB (left) merge into a continuous helix at the Smc neck in *B. subtilis* SmcHead–ScpA^{N} (right).

structure. Upon binding Smc, this segment undergoes a pronounced structural change to form a single α-helix (**Fig. 3f**). The long helix displays extensive interactions with both αN and αC helices of the Smc neck, which together form a three-stranded coiled coil (**Fig. 3e**). Side chains of Smc residues Tyr170 and Val1021—shown to be important for binding ScpA^{N}—are located in the hydrophobic core of the interface (**Fig. 3e**), which explains the detrimental effect of their substitution to glutamate. Furthermore, Arg1032 in Smc is positioned in proximity to ScpA's Val50 and Glu52, as expected from cross-linking of cysteine mutants (**Fig. 3e**). The presented structure of Smc–ScpA^{N} probably closely resembles its architecture *in vivo*.

We next selected conserved residues in ScpA that are located at or near the Smc–ScpA^{N} interface and mutated them to lysine or glutamate. Three mutations (L60K, L67E and K70E) resulted in *scpA*-null phenotypes and interfered with binding of recombinant ScpA^{ΔC}–ScpB to SmcHead (**Supplementary Fig. 3b–d**). Side chains of these residues are in direct contact with the Smc neck, which implies that their mutation disrupts the interface (**Supplementary Fig. 3e**).

Modeling possible Smc–ScpAB holocomplexes

To obtain a view of the overall architecture, we modeled Smc–ScpAB complexes on the basis of the three determined structures. First, we superimposed two copies of BsSmcHead–ScpA^{N} onto the dimer of *P. furiosus* (Pf) SmcHead–ScpA^{C}. Noting that the exposed side of α3 in *S. pneumoniae* (Sp) ScpA^{ΔC}–ScpB is in contact with the Smc neck in the BsSmcHead–ScpA^{N} structure (**Fig. 3f**), we superimposed the corresponding segments of the SpScpA^{ΔC}–ScpB structure and the SmcHead–ScpA^{N}–ScpA^{C} model. We found that overlaps could be removed by rigid body movements of helix α1 and the central part of SpScpA^{ΔC}–ScpB, assuming flexibility in the α1-α2 and α3-α4 loops of ScpA. In this way, ScpA^{ΔC} could be connected to either copy of ScpA^{C} by fewer than 14 residues, the expected number of amino acids in the ScpA linker segment. ScpA might therefore bridge two distinct Smc proteins or bind both sites of a single Smc (**Fig. 4a**). Thus, modeling failed to unambiguously resolve the shape and stoichiometry of Smc–ScpAB *in vivo*.

Stoichiometry of Smc–ScpAB complexes in cells

To test how many binding sites on Smc dimers are occupied *in vivo* and to determine how they are interconnected by ScpAB, we performed a number of biochemical and genetic experiments.

First, we probed the organization of Smc–ScpAB in *B. subtilis* cells by simultaneous cross-linking at the neck and cap interface. Depending on the prevalent architecture (**Fig. 4b**), possible cross-linked products are the Smc$_2$–ScpA$_2$, Smc–ScpA$_2$ and Smc–ScpA–Smc species as well as a 'Smc=ScpA' product in which both ends of kleisin are

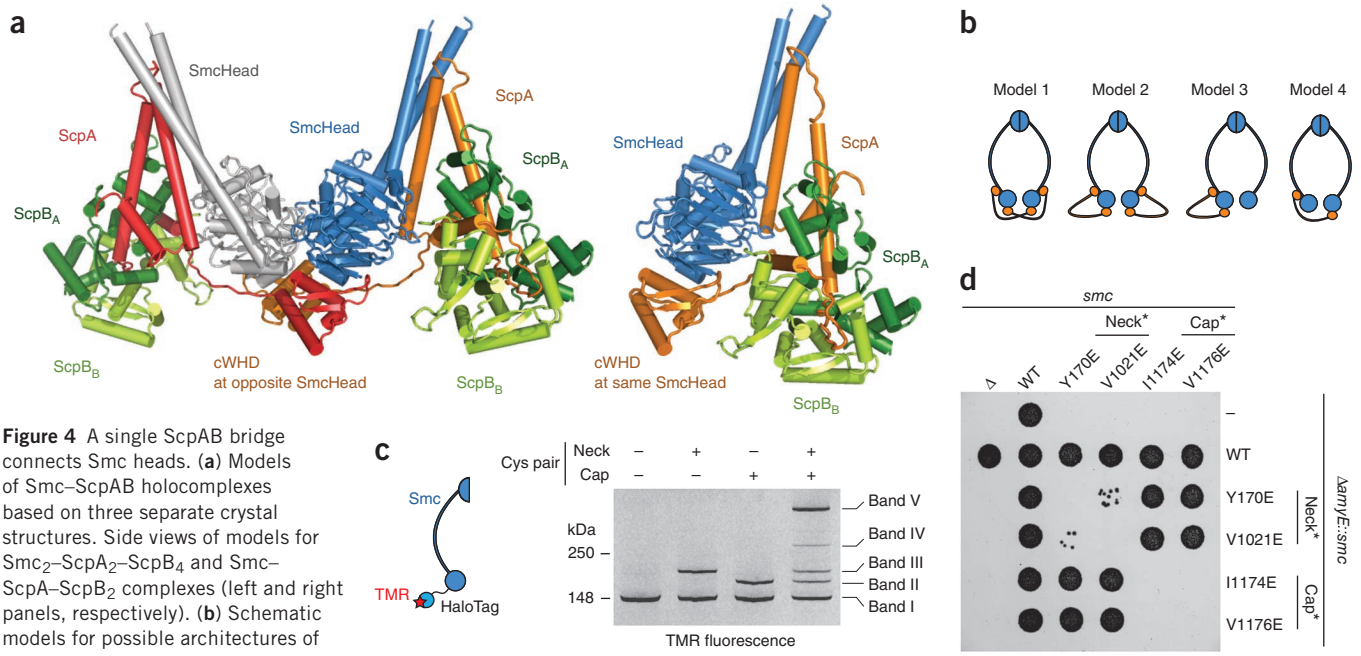

Figure 4 A single ScpAB bridge connects Smc heads. (**a**) Models of Smc–ScpAB holocomplexes based on three separate crystal structures. Side views of models for Smc_2–$ScpA_2$–$ScpB_4$ and Smc–ScpA–$ScpB_2$ complexes (left and right panels, respectively). (**b**) Schematic models for possible architectures of Smc–ScpA complexes. (**c**) Analysis of cross-linked products of Smc–ScpA formed in *B. subtilis*. Strains BSG689 and BSG728-730 were cross-linked at the indicated interfaces with BMOE, and the levels of Smc-HaloTag species were quantified in SDS PAGE gels by detection of a TMR label attached to the HaloTag, as shown. (**d**) Growth assay of *B. subtilis* strains carrying two alleles of *smc*. Cells were spotted on nutrient agar (NA) plates and incubated at 37 °C (strain numbers are given in **Supplementary Fig. 4d**).

cross-linked to the same Smc molecule. We created strains containing Smc-HaloTag and cysteine pairs at either one or both interfaces and quantified cross-linked products by in-gel fluorescence, using a HaloTag TMR substrate. Cells that were cross-linkable at both cap and neck interfaces yielded an additional species with high apparent molecular weight (**Fig. 4c**, band V) and a minor medium-sized band (band IV). To determine the composition of these cross-linked species, we first quantified the cross-linking reaction by chemical kinetic modeling (details given in **Supplementary Note**). This allowed prediction of the reaction outcome on the basis of single cross-link efficiencies, assuming a homogenous starting population of complexes. Notably, only in the case of presumed Smc–ScpA–Smc complexes (**Fig. 4b**, model 4) were relative amounts of all products correctly predicted within the s.d. (**Table 2**). Next, we estimated the Smc/ScpA ratio in the observed products by MS (**Supplementary Fig. 4a**). LC-MS analysis indicated a 1:1 stoichiometry of Smc and ScpA in band IV and a higher ratio of Smc to ScpA (1.44:1) in band V, consistent with a 2:1 stoichiometry. These findings indicated that the major species (band V) is derived from Smc dimers bridged by a single ScpA subunit and the minor species (band IV) from Smc proteins connected at two interfaces to a single ScpA. Consistent with this notion, Smc deficient in dimerization at the hinge domain[35] generated high levels of band IV and low levels of band V (**Supplementary Fig. 4b**). Finally, we tested whether these high–molecular weight species contain more than one ScpA subunit. To do so, we constructed strains containing ectopic epitope-tagged and endogenous untagged ScpA with one and two cysteine residues, respectively. ScpA with a single cysteine mutation was never detected in bands IV and V despite the presence of these species in the same cells, which demonstrates that the cross-linked products do not contain more than a single copy of ScpA (**Supplementary Fig. 4c**). These results clearly establish that only one ScpA is bound to Smc at any one time and reveal that a single ScpA bridges two Smc proteins in the majority of complexes.

Notably, the lethality of Smc neck mutations was suppressed by the presence of ectopic cap mutant Smc, and cap mutations were likewise suppressed by ectopic neck mutants (**Fig. 4d**), which strongly supports that Smc_2–ScpA is the functional core complex. Thus, a single binding site each for the N and C termini of ScpA per Smc dimer is sufficient for Smc–ScpAB activity.

SMC–kleisin rings versus SMC–kleisin chains

Smc dimers binding ScpA subunits could form tripartite rings or oligomeric chains (**Fig. 5a**). However, viability supported by mixtures of cap- and neck-mutant Smc proteins (**Fig. 4d**) indicates that tripartite rings are the functionally relevant structure. A strictly alternating assembly of mutants into chains seems improbable but might still be possible. Therefore, we aimed to detect these structures *in vivo* by simultaneous cross-linking at cap, neck and hinge interfaces. We introduced a pair of cysteines into the Smc hinge for efficient cross-linking (**Supplementary Fig. 5a**) and then combined cysteines at the hinge with cysteines at Smc–ScpA interfaces in Smc-HaloTag. Cross-linking generated a major low-mobility species corresponding to Smc–ScpA–Smc polypeptides with cross-linked hinges (**Fig. 5a**). Notably, bands with higher apparent molecular weight were not observed. We confirmed this finding with untagged strains by immunoblotting (**Supplementary Fig. 5b**). Thus, in addition to the genetic data, the absence of very large cross-linked entities suggests that condensin in *B. subtilis* rarely or never exists as SMC–kleisin chains *in vivo*. In general, N- and C-terminal domains of ScpA connect the heads of a Smc dimer to form asymmetric tripartite rings.

An asymmetric architecture critical for Smc–ScpAB function

To investigate whether the observed stoichiometry and the interrelated asymmetry are crucial for proper function, we artificially transformed Smc_2–ScpA into Smc_2–$ScpA_2$ structures by fusing every Smc in the cell to ScpA. To do so, we relocated the *scpA* gene to the *smc* locus and

Table 2 Quantification of Smc-ScpA products cross-linked at cap and neck

	Fraction of intensity				
	Prediction				Experiment
	Model 1	Model 2	Model 3	Model 4	Mean ± s.d
Band I	0.49	0.49	0.58	0.40	0.43 ± 0.08
Band II	0.15	0.21	0.12	0.12	0.12 ± 0.03
Band III	0.15	0.21	0.12	0.12	0.10 ± 0.02
Band IV	–	–	–	–	0.02 ± 0.01
Band V	0.21	0.09	0.18	0.36	0.33 ± 0.08

Relative amounts of cross-linked species predicted (on the basis of models 1–4) and experimentally determined (**Fig. 4c**). Means and s.d. of experimental values were determined from three independent replicates.

connected its N terminus by a linker to *smc* (**Fig. 5b**). The resulting strain produced the fusion (Smc-ScpA) as the sole source of Smc and ScpA. This fusion protein was not functional (**Fig. 5b**) despite being expressed at normal levels (**Supplementary Fig. 5c**). This indicates that Smc-ScpA cannot fold properly, this fusion interferes with an unknown function or symmetric complexes are nonfunctional. Notably, the presence of an ectopic copy of wild-type Smc but not ScpA rescued growth of the fusion strain (**Fig. 5b**). Crucially, the fusion also supported viability when the ectopic *smc* gene contained a neck mutation (Y170E or V1021E) but not when it was exchanged for cap mutants (I1174E or V1176E). These findings indicate that Smc-ScpA regains functionality when it forms asymmetric complexes with free Smc. Similar results were obtained when the genetic locations of *smc* and *smc-scpA* genes were reciprocally exchanged (**Supplementary Fig. 5d**). Next, we created another type of symmetric SMC–kleisin complex by connecting the C terminus of ScpA to Smc (ScpA-Smc). In contrast to the results with the Smc-ScpA fusion, the functionality of this protein was rescued by cap- but not neck-mutant Smc (**Fig. 5b**). Finally, the function of ScpA-Smc was affected by a mutation in its cap, whereas that of Smc-ScpA was impaired by a mutation in its neck (**Supplementary Fig. 5e**,**f**), which indicates that these interfaces do not merely connect ScpA and Smc but serve additional essential and probably distinct functions.

From this, we conclude that fusion of ScpA and Smc does not interfere with activity, provided that the fusion protein can form asymmetric complexes. Together, our findings demonstrate that binding of a single ScpA subunit to Smc dimers is sufficient for normal activity and that artificial recruitment of a second ScpA subunit to the complex is detrimental.

Assembling asymmetrically bridged Smc–ScpAB

Smc–ScpAB adopts an asymmetric structure with a single ScpAB bridging the heads of a Smc dimer (**Fig. 4b**, model 4). However, *in vitro*, single SmcHeads can readily be occupied by $ScpA^N$ and $ScpA^C$ at the same time (**Supplementary Fig. 6a**,**b**). It therefore seems unlikely that a conformational change induced at one interface precludes binding at the other. Alternative mechanisms must exist to prevent incorporation of excess kleisin subunits. To investigate a possible interdependence in the formation of Smc-nαHD and Smc-cWHD interactions, we monitored binding at one interface *in vivo* by cysteine cross-linking while the other was blocked by mutation. Notably, we found that cross-linking of cWHD to the Smc cap was abolished by mutations in the Smc neck (**Fig. 6a**) as well as mutations in the nαHD of ScpA (**Supplementary Fig. 6c**). Likewise, cross-linking of ScpA's nαHD to the neck was largely diminished in Smc cap mutants (**Fig. 6a**). Together, these results indicate that the interactions of the Smc neck and cap with ScpA are interdependent *in vivo*. It is likely that ScpAB is only transiently associated with Smc through a single interface *in vivo*.

It was previously shown *in vitro* that ATP-dependent engagement of MukB heads releases one of two bound MukF cWHDs, owing to steric hindrance[29]. An analogous mechanism could explain how a second

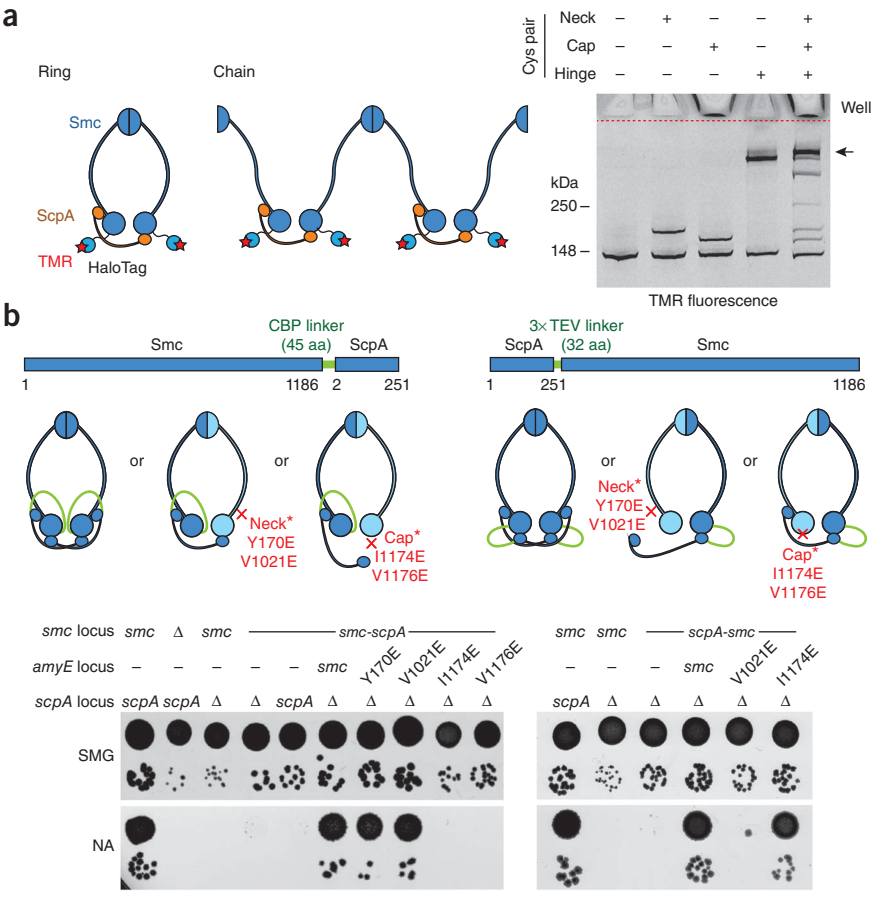

Figure 5 Architecture of Smc–ScpAB complexes *in vivo*. (**a**) Detection of Smc protein species after simultaneous cross-linking of three interfaces in Smc-ScpAB using Smc-HaloTag. Strains BSG689, BSG728-729 and BSG1077-1078 were grown in LB medium and processed as described in **Figure 4c**. The arrow indicates a band containing hinge-linked Smc dimers cross-linked to ScpA. (**b**) Colony-formation assay with strains carrying *smc-scpA* or *scpA-smc* gene fusions. Schematic depiction of Smc-ScpA and ScpA-Smc fusion proteins and their complexes with mutant Smc proteins (top). Strains BSG1, BSG68, BSG397, BSG398, BSG396, BSG708–BSG710, BSG737 and BSG738 (bottom left) and strains BSG1004, BSG1005, BSG1039 and BSG1042–1044 (bottom right), assayed for growth as in **Figure 1c** are shown. aa, amino acids.

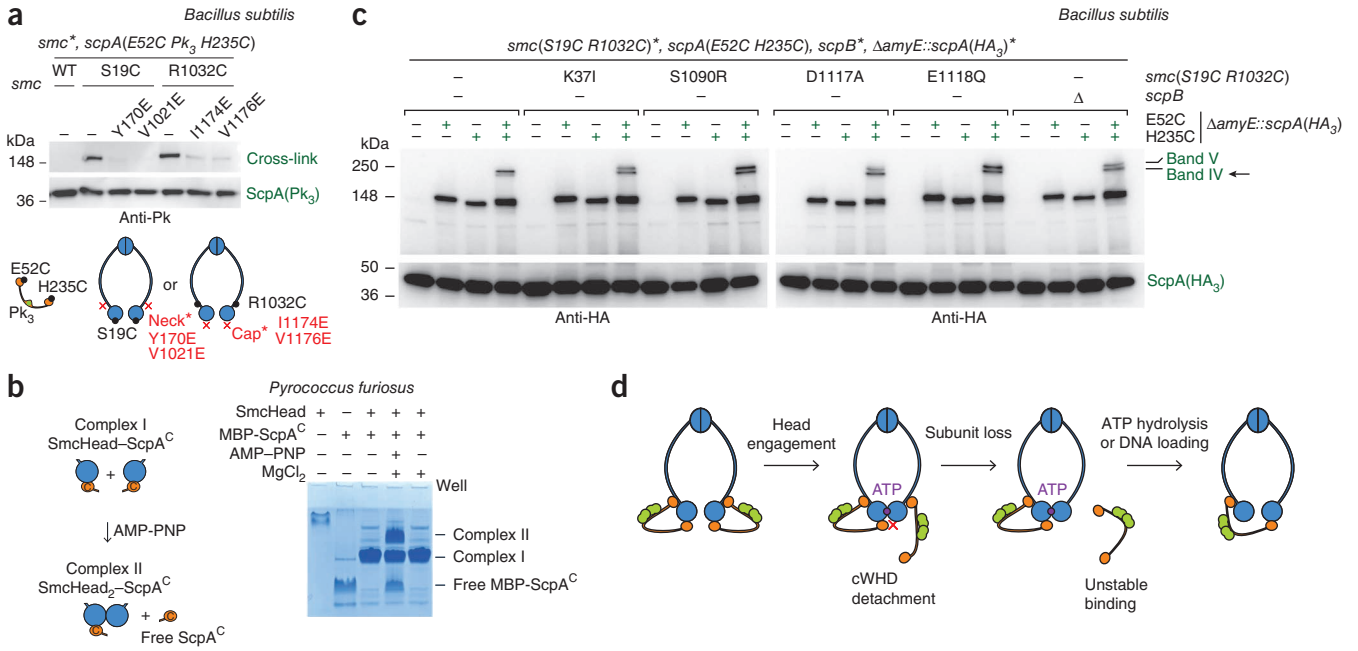

Figure 6 Mechanisms promoting assembly of Smc_2–ScpA–$ScpB_2$ rings. (**a**) Detection of cysteine cross-linking at the Smc neck–ScpA interface in cap-mutant proteins and at the Smc cap–ScpA interface in neck-mutant proteins. ScpA and its cross-linked products, detected by immunoblotting using anti-Pk antibodies, are shown for *B. subtilis* strains BSG534 and BSG859–BSG864 grown in minimal medium and incubated with either DMSO alone (–) or BMOE (+). (**b**) Native PAGE analysis of purified SmcHead–$ScpA^C$ complexes in the presence of nucleotide. Purified fractions of *P. furiosus* SmcHead and MBP–$ScpA^C$ mixed with and without AMP-PNP are shown analyzed by native PAGE and Coomassie staining. (**c**) Analysis of Smc-ScpA interactions by cysteine cross-linking in cells that lack ScpB or are deficient in the Smc ATP-hydrolysis cycle. Cells of strains BSG649–652 and BSG953–972 were cross-linked with BMOE and analyzed by immunoblotting using anti-HA antibodies as shown. HA_3, triple HA tag. The band marked by an arrow comprises a ScpA subunit cross-linked twice to a single Smc protein. K37I and D1117A prevent ATP binding, S1090R prevents head engagement, and E1118Q prevents ATP hydrolysis. (**d**) Schematic model for the transformation of symmetric into asymmetric Smc–ScpAB complexes.

ScpAB is excluded from Smc–ScpAB complexes. To test this possibility, we mixed purified PfSmcHead with MBP-tagged $PfScpA^C$ in the absence or presence of the nonhydrolyzable ATP analog AMP-PNP. Reaction products were analyzed by native PAGE, revealing a substantial loss of $PfScpA^C$ from engaged Smc heads (**Fig. 6b**). This result was confirmed with untagged $PfScpA^C$ and PfScpA (**Supplementary Fig. 6d**). However, we were unable to measure cWHD detachment by using protein fragments from *B. subtilis* or *S. pneumoniae*, possibly because of a more transient association of the respective proteins (data not shown). As is the case in MukBEF, detachment of $PfScpA^C$ from PfSmcHead *in vitro* was dependent on the linker segment preceding the cWHD (data not shown), which suggests that this segment might occlude the cap of the second Smc head. However, when head engagement is driven by high protein concentration (that is, during crystallization) rather than by nucleotide binding, each Smc head can associate with a cWHD (**Fig. 1b**). Under these conditions, cWHDs might successfully compete with the linker segment for binding to the second Smc cap. Taken together, cooperative binding of nαHD and cWHD as well as occlusion of both caps might be sufficient to prevent stable association of a second ScpAB with Smc dimers.

In vivo a small fraction of Smc–ScpAB comprises ScpA subunits bound to the neck and cap of the same Smc head (**Fig. 4b**, models 2 and 3). These Smc=ScpA complexes are probably not relevant for function, as cap and neck mutants are reciprocally complemented (**Fig. 4d**). Possibly, mechanisms exist that help to transform these structures into asymmetrically bridged Smc–ScpAB. Notably, using cross-linking we found that Smc–ScpA complexes that are deficient in ATP hydrolysis or lack the ScpB subunit form substantial amounts of Smc=ScpA complexes (band IV) *in vivo* (**Fig. 6c**). This might indicate that aberrant complexes are selectively destabilized during the ATP-hydrolysis cycle in a manner dependent on ScpB (**Fig. 6d**). Alternatively, correct assembly of asymmetric Smc–ScpAB rings might be linked, for example, to their loading onto DNA, a process probably dependent on ATP hydrolysis and on ScpB[33,36]. Of note, even in the absence of ScpB or ATP binding no more than one ScpA associated with a given Smc protein (**Fig. 6c**), which suggests that doubly bridged Smc dimers (**Fig. 4b**, model 1) cannot form even under these conditions.

DISCUSSION

Identical molecules with mutually exclusive roles

Three interfaces on Smc proteins are required for formation of functional SMC–kleisin complexes in *B. subtilis*: the hinge domain, which mediates dimerization of Smc proteins, and the Smc cap and neck regions, which bind N- and C-terminal domains of ScpA, respectively. Crucially, the two Smc proteins in a tripartite Smc_2–ScpA complex have unique roles: the first, henceforth named κ-Smc protein ('kappa' for cap-protein association), binds the cWHD of ScpA, whereas the second, called ν-Smc ('nu' for neck interface), forms a three-stranded coiled coil together with the N terminus of ScpA (**Fig. 7**). Smc proteins have to adopt their mutually exclusive roles upon binding to ScpAB. We postulate that a molecular mechanism based on steric occlusion and cooperative binding operates to ensure the attachment of a single ScpAB to Smc dimers (**Fig. 6d**).

In contrast, eukaryotic genomes encode specialized κ-SMC proteins, such as cohesin's Smc1 and condensin's Smc4, and specialized ν-SMC proteins, such as cohesin's Smc3 and condensin's Smc2. The latter SMC proteins might also form three-stranded coiled coils together with the N termini of their kleisin subunits. It is likely that

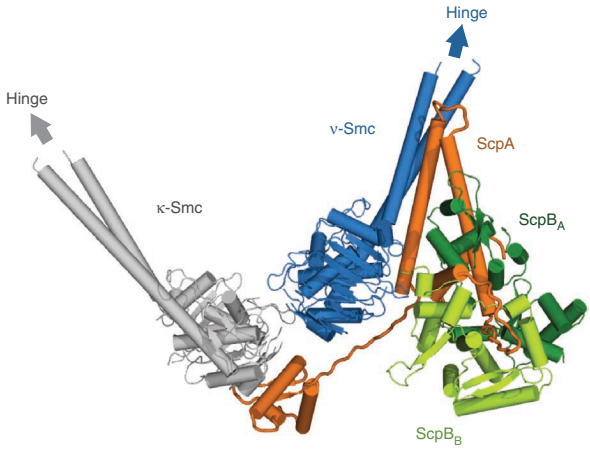

Figure 7 Model for the functional unit of the Smc–ScpAB holocomplex in cells. The asymmetric Smc_2–ScpA–$ScpB_2$ complex with nucleotide-free head domains is shown.

duplication and divergence of SMC genes early in the evolution of eukaryotes have eliminated dual-role SMC proteins, thereby increasing flexibility in the regulation of SMC activity, for example by specific acetylation of Smc3 protein in cohesin or by binding of Mms21 specifically to the Smc5 coiled coil[37–39].

Monomeric versus dimeric kleisin bridges

Our study revealed that the structure of ScpAB is very different from that of MukEF. Because of its symmetric nature, MukF bridges MukB by interacting with the cap regions of two MukB heads, thus producing symmetric rings or higher-order assemblies. Notably, the two MukB head domains bridged by MukF are unable to engage with one another, as they are separated by ~170 Å (ref. 29). Probably, larger structures that contain more than one MukB dimer are the functional units *in vivo*. Consistent with this idea, quantitative microscopic analysis of fluorescent MukBEF foci has revealed that the minimal unit of MukBEF in *E. coli* is probably formed by two MukB dimers held together by a single $MukE_4F_2$ subcomplex[31]. In contrast, the two Smc head domains bridged by ScpAB are close to each other in our models and are thus probably able to undergo the ATPase cycle. We show that, consistent with the short kleisin bridge, tripartite Smc–ScpAB rings are the functional unit *in vivo*. However, our results do not exclude the formation of higher-order structures through unknown interfaces or binding partners. It appears that at some point in evolution MukBEF has transformed its kleisin bridge from a monomer to a dimer and concurrently lost its ν-SMC activity. This might have triggered rapid divergent evolution from other SMC proteins[40].

Asymmetry in opening the DNA entry and exit gates

Currently, a precise function of the overall asymmetry in canonical SMC complexes seems enigmatic. However, we speculate that the inherent asymmetry found in cohesin and prokaryotic condensin is coupled to a conserved molecular mechanism using ATP binding and hydrolysis to drive ring opening. In cohesin, the SMC hinge domain and the Smc3–Scc1 interface probably serve as entry and exit gates for DNA, respectively[41,42]. How opening of the ring is achieved is currently poorly understood. However, binding and hydrolysis of ATP by SMC proteins is essential for DNA loading and has been suggested to provide the energy for transient detachment of the hinge[22–24,41]. In prokaryotic condensin, the binding of ScpA to Smc dimers presumably forces the head domains into different configurations, owing to their association with opposite ends of the kleisin subunit. ATP binding or hydrolysis might thus trigger distinct conformational changes in the two head domains that could act synergistically to open the tripartite ring for DNA entry. For example, the coiled coils emanating from the Smc heads could twist into opposite directions upon head engagement. In the case of a rigid coiled coil connecting the Smc head and hinge, a torque would be generated at the hinge that could trigger transient detachment. In this respect, it seems of utmost importance to dissect which other parts of Smc proteins have asymmetric requirements during DNA loading or unloading.

Asymmetry could also be relevant for the opening of a proposed DNA-exit gate at the SMC–$kleisin^N$ interface. In cohesin $Scc1^N$ presumably detaches frequently from the Smc3 head, thus leading to turnover on chromosomes until acetylation of the Smc3 head by Eco1 prevents Smc3–Scc1 detachment[42]. Similarly, $ScpA^N$ could transiently detach from the Smc neck to allow release of the DNA from the prokaryotic condensin ring. In the case of asymmetric complexes, only a single interface has to detach to create an opening in the ring. Such an exit gate would not have essential roles, at least in *B. subtilis* (as with cohesin in yeast[41]) because covalent fusion of the N terminus of ScpA to Smc creates a functional protein (**Fig. 5b**). Notably, we observed a different conformation of $ScpA^N$ bound to the Smc neck compared to its free form (**Fig. 3f**). Mechanisms that revert the bound form of $ScpA^N$ back into a free nαHD, for example by breakage of the α(2–3) helix, could thus promote detachment of $kleisin^N$ from SMC in prokaryotic condensin as well as in cohesin.

As an alternative that is not mutually exclusive with the models proposed above, asymmetry in SMC–kleisin complexes might induce distinct geometries in DNA or facilitate their recognition, as has recently been considered as a unifying principle for SMC protein function[43].

In summary, Smc–ScpAB complexes form asymmetric tripartite rings, similar in shape and size to cohesin. All three interfaces and the overall organization of SMC–kleisin rings seem to be conserved between prokaryotic condensin and its eukaryotic cousins. We presume that all related complexes including cohesins and condensins might act as DNA tethers that entrap DNA fibers by using fundamentally conserved mechanisms.

METHODS

Methods and any associated references are available in the online version of the paper.

Accession codes. Coordinates of SmcHead–$ScpA^C$, $ScpA^{\Delta C}$–ScpB and SmcHead–$ScpA^N$ together with structure factors have been deposited at the Protein Data Bank, with accession numbers 4I99, 4I98 and 3ZGX, respectively.

Note: Supplementary information is available in the online version of the paper.

ACKNOWLEDGMENTS

We thank E. Conti and S. Jentsch for sharing resources and helpful advice and K. Nasmyth and W. Zachariae for critical reading of the manuscript. We are grateful to the MPI Crystallization Facility for HTP screening, to the MPI Core Facility and C. Eberl for help with MS analysis, to M. Blettinger, A.-L. Cost and P. Ringer for technical help and to H. Murray (Newcastle University, Newcastle upon Tyne, UK) for providing DnaA protein and antiserum. S. Uebel kindly performed and analyzed the analytical ultracentrifugation experiments. We thank A. Pauluhn, V. Olieric and the staff of the PX beamlines at the Swiss Light Source (SLS, Villigen, Zurich) for assistance during crystallographic data collection and E. Lorentzen and R. Prabu for helpful advice for twinning refinement. We also acknowledge the use of Beamline 5C at PAL and BL41XU at the SPring-8. This work was supported by funding from the Max Planck Society and a Starting Grant from the European Research Council ERC StG #260853 "DiseNtAngle" (S.G.) and by the National Research Foundation of Korea grant 2012-0005612 (B.-H.O.).

AUTHOR CONTRIBUTIONS
F.B., *B. subtilis* strain constructions and cellular and biochemical experiments; H.-C.S., F.B., Y.-M.S. and V.G.-O., protein purification; H.-C.S. and Y.-M.S., structure determination and biochemical experiments; J.B. and Y.-G.K., X-ray data collection and structure determination; F.B., H.-C.S., S.G. and B.-H.O. conception of experiments and preparation of the manuscript.

COMPETING FINANCIAL INTERESTS
The authors declare no competing financial interests.

Published online at http://www.nature.com/doifinder/10.1038/nsmb.2488.
Reprints and permissions information is available online at http://www.nature.com/reprints/index.html.

1. Hirano, T. At the heart of the chromosome: SMC proteins in action. *Nat. Rev. Mol. Cell Biol.* **7**, 311–322 (2006).
2. Nasmyth, K. & Haering, C.H. Cohesin: its roles and mechanisms. *Annu. Rev. Genet.* **43**, 525–558 (2009).
3. Cuylen, S. & Haering, C.H. Deciphering condensin action during chromosome segregation. *Trends Cell Biol.* **21**, 552–559 (2011).
4. D'Ambrosio, C., Kelly, G., Shirahige, K. & Uhlmann, F. Condensin-dependent rDNA decatenation introduces a temporal pattern to chromosome segregation. *Curr. Biol.* **18**, 1084–1089 (2008).
5. Fousteri, M.I. & Lehmann, A.R. A novel SMC protein complex in *Schizosaccharomyces pombe* contains the Rad18 DNA repair protein. *EMBO J.* **19**, 1691–1702 (2000).
6. Kegel, A. *et al.* Chromosome length influences replication-induced topological stress. *Nature* **471**, 392–396 (2011).
7. Mascarenhas, J., Soppa, J., Strunnikov, A.V. & Graumann, P.L. Cell cycle-dependent localization of two novel prokaryotic chromosome segregation and condensation proteins in *Bacillus subtilis* that interact with SMC protein. *EMBO J.* **21**, 3108–3118 (2002).
8. Soppa, J. *et al.* Discovery of two novel families of proteins that are proposed to interact with prokaryotic SMC proteins, and characterization of the *Bacillus subtilis* family members ScpA and ScpB. *Mol. Microbiol.* **45**, 59–71 (2002).
9. Britton, R.A., Lin, D.C. & Grossman, A.D. Characterization of a prokaryotic SMC protein involved in chromosome partitioning. *Genes Dev.* **12**, 1254–1259 (1998).
10. Hirano, M. & Hirano, T. Positive and negative regulation of SMC-DNA interactions by ATP and accessory proteins. *EMBO J.* **23**, 2664–2673 (2004).
11. Niki, H., Jaffe, A., Imamura, R., Ogura, T. & Hiraga, S. The new gene mukB codes for a 177 kd protein with coiled-coil domains involved in chromosome partitioning of *E. coli*. *EMBO J.* **10**, 183–193 (1991).
12. Yamazoe, M. *et al.* Complex formation of MukB, MukE and MukF proteins involved in chromosome partitioning in *Escherichia coli*. *EMBO J.* **18**, 5873–5884 (1999).
13. Gruber, S. & Errington, J. Recruitment of condensin to replication origin regions by ParB/SpoOJ promotes chromosome segregation in *B. subtilis*. *Cell* **137**, 685–696 (2009).
14. Minnen, A., Attaiech, L., Thon, M., Gruber, S. & Veening, J.W. SMC is recruited to oriC by ParB and promotes chromosome segregation in *Streptococcus pneumoniae*. *Mol. Microbiol.* **81**, 676–688 (2011).
15. Sullivan, N.L., Marquis, K.A. & Rudner, D.Z. Recruitment of SMC by ParB-parS organizes the origin region and promotes efficient chromosome segregation. *Cell* **137**, 697–707 (2009).
16. Danilova, O., Reyes-Lamothe, R., Pinskaya, M., Sherratt, D. & Possoz, C. MukB colocalizes with the oriC region and is required for organization of the two *Escherichia coli* chromosome arms into separate cell halves. *Mol. Microbiol.* **65**, 1485–1492 (2007).
17. Griese, J.J., Witte, G. & Hopfner, K.P. Structure and DNA binding activity of the mouse condensin hinge domain highlight common and diverse features of SMC proteins. *Nucleic Acids Res.* **38**, 3454–3465 (2010).
18. Haering, C.H., Lowe, J., Hochwagen, A. & Nasmyth, K. Molecular architecture of SMC proteins and the yeast cohesin complex. *Mol. Cell* **9**, 773–788 (2002).
19. Kurze, A. *et al.* A positively charged channel within the Smc1/Smc3 hinge required for sister chromatid cohesion. *EMBO J.* **30**, 364–378 (2011).
20. Haering, C.H. *et al.* Structure and stability of cohesin's Smc1-kleisin interaction. *Mol. Cell* **15**, 951–964 (2004).
21. Lammens, A., Schele, A. & Hopfner, K.P. Structural biochemistry of ATP-driven dimerization and DNA-stimulated activation of SMC ATPases. *Curr. Biol.* **14**, 1778–1782 (2004).
22. Arumugam, P. *et al.* ATP hydrolysis is required for cohesin's association with chromosomes. *Curr. Biol.* **13**, 1941–1953 (2003).
23. Weitzer, S., Lehane, C. & Uhlmann, F. A model for ATP hydrolysis-dependent binding of cohesin to DNA. *Curr. Biol.* **13**, 1930–1940 (2003).
24. Hu, B. *et al.* ATP hydrolysis is required for relocating cohesin from sites occupied by its Scc2/4 loading complex. *Curr. Biol.* **21**, 12–24 (2011).
25. Schleiffer, A. *et al.* Kleisins: a superfamily of bacterial and eukaryotic SMC protein partners. *Mol. Cell* **11**, 571–575 (2003).
26. Gruber, S., Haering, C.H. & Nasmyth, K. Chromosomal cohesin forms a ring. *Cell* **112**, 765–777 (2003).
27. Haering, C.H., Farcas, A.M., Arumugam, P., Metson, J. & Nasmyth, K. The cohesin ring concatenates sister DNA molecules. *Nature* **454**, 297–301 (2008).
28. Ivanov, D. & Nasmyth, K. A topological interaction between cohesin rings and a circular minichromosome. *Cell* **122**, 849–860 (2005).
29. Woo, J.S. *et al.* Structural studies of a bacterial condensin complex reveal ATP-dependent disruption of intersubunit interactions. *Cell* **136**, 85–96 (2009).
30. Fennell-Fezzie, R., Gradia, S.D., Akey, D. & Berger, J.M. The MukF subunit of *Escherichia coli* condensin: architecture and functional relationship to kleisins. *EMBO J.* **24**, 1921–1930 (2005).
31. Badrinarayanan, A., Reyes-Lamothe, R., Uphoff, S., Leake, M.C. & Sherratt, D.J. In vivo architecture and action of bacterial structural maintenance of chromosome proteins. *Science* **338**, 528–531 (2012).
32. Fuentes-Perez, M.E., Gwynn, E.J., Dillingham, M.S. & Moreno-Herrero, F. Using DNA as a fiducial marker to study SMC complex interactions with the atomic force microscope. *Biophys. J.* **102**, 839–848 (2012).
33. Volkov, A., Mascarenhas, J., Andrei-Selmer, C., Ulrich, H.D. & Graumann, P.L. A prokaryotic condensin/cohesin-like complex can actively compact chromosomes from a single position on the nucleoid and binds to DNA as a ring-like structure. *Mol. Cell. Biol.* **23**, 5638–5650 (2003).
34. Kim, J.S. *et al.* Crystal structure and domain characterization of ScpB from *Mycobacterium tuberculosis*. *Proteins* **71**, 1553–1556 (2008).
35. Hirano, M. & Hirano, T. Hinge-mediated dimerization of SMC protein is essential for its dynamic interaction with DNA. *EMBO J.* **21**, 5733–5744 (2002).
36. Mascarenhas, J. *et al.* Dynamic assembly, localization and proteolysis of the *Bacillus subtilis* SMC complex. *BMC Cell Biol.* **6**, 28 (2005).
37. Stephan, A.K., Kliszczak, M. & Morrison, C.G. The Nse2/Mms21 SUMO ligase of the Smc5/6 complex in the maintenance of genome stability. *FEBS Lett.* **585**, 2907–2913 (2011).
38. Unal, E. *et al.* A molecular determinant for the establishment of sister chromatid cohesion. *Science* **321**, 566–569 (2008).
39. Rolef Ben-Shahar, T. *et al.* Eco1-dependent cohesin acetylation during establishment of sister chromatid cohesion. *Science* **321**, 563–566 (2008).
40. Gruber, S. MukBEF on the march: taking over chromosome organization in bacteria? *Mol. Microbiol.* **81**, 855–859 (2011).
41. Gruber, S. *et al.* Evidence that loading of cohesin onto chromosomes involves opening of its SMC hinge. *Cell* **127**, 523–537 (2006).
42. Chan, K.L. *et al.* Cohesin's DNA exit gate is distinct from its entrance gate and is regulated by acetylation. *Cell* **150**, 961–974 (2012).
43. Carter, S.D. & Sjogren, C. The SMC complexes, DNA and chromosome topology: right or knot? *Crit. Rev. Biochem. Mol. Biol.* **47**, 1–16 (2012).

ONLINE METHODS

***Bacillus subtilis* strains and media.** Genetic modifications of *smc*, *scpAB* and *amyE* loci in *B. subtilis* 168 were done by double-crossover recombination. Genotypes are listed in **Supplementary Table 2**. Transformation of competent *B. subtilis* cells was performed by a two-step starvation protocol using competence medium for growth as previously described[44] with minor modifications. Briefly, cells were grown overnight in 5 ml competence medium, that is, SMM solution (15 mM ammonium sulfate, 80 mM dipotassium hydrogen phosphate, 44 mM potassium dihydrogen phosphate, 3.4 mM trisodium citrate, 0.8 mM magnesium sulfate 6 g l^{-1} potassium hydrogen phosphate) supplemented with 5 g l^{-1} glucose, 20 mg l^{-1} tryptophan, 20 mg l^{-1} casamino acids, 6 mM magnesium sulfate and 110 mg l^{-1} ferric ammonium citrate. Of this culture, 600 µl were diluted into 10 ml fresh competence medium. Cells were grown for 3 h at 37 °C, then diluted with 10 ml prewarmed starvation medium (SMM supplemented with 5 g l^{-1} glucose and 6 mM magnesium sulfate) and incubated for 1 h at 37 °C. Cells (400 µl) were mixed with DNA, incubated for 2 h at 37 °C and plated on appropriate selection media. Selection of *B. subtilis* strains was done on nutrient agar plates (Oxoid) supplemented as required with 5 µg ml^{-1} chloramphenicol, 3 µg ml^{-1} kanamycin, 50 µg ml^{-1} spectinomycin, 15 µg ml^{-1} tetracycline, 0.5 µg ml^{-1} erythromycin and 12.5 µg ml^{-1} lincomycin. Cells showing *smc*, *scpA* or *scpB* phenotypes were selected on SMG medium, that is, SMM solution supplemented with glucose (5 g l^{-1}), tryptophan (20 mg l^{-1}) and glutamate (1 g l^{-1}). After selection and single-colony purification, strains generated by double crossover were grown in the absence of antibiotics. Prokaryotic condensin cysteine derivatives and *scpA*(Pk_3), *scpA*(HA_3), *smc-HaloTag* and *smc-*His_{12} alleles were functional as judged by their ability to support growth at 37 °C on rich media.

Production and purification of recombinant proteins. Expression constructs (**Supplementary Table 3**) were prepared in pET-28 derived plasmids by Golden-Gate cloning[45] or in other plasmids by standard PCR-based cloning methods. All recombinant proteins were produced in *E. coli* BL21 (DE3), BL21-Gold (DE3) or BL21 (DE3)-RIPL strains (Novagen). Protein complexes were obtained by coexpression or by mixing components and were purified by using metal-affinity, ion-exchange and size-exclusion chromatography.

Crystallization and X-ray structure determination. Selenomethionine (SeMet)-labeled *P. furiosus* SmcHead–$ScpA^C$ (10 mg ml^{-1}) was crystallized in 220 mM ammonium phosphate dibasic, 16% polyethylene glycol 3350 and 100 mM Bicine pH 9.0; SeMet-labeled *S. pneumoniae* $ScpA^{\Delta C}$–ScpB (20 mg ml^{-1}) in 200 mM trimethylamine N-oxide, 20% polyethylene glycol monomethyl ether 2000 and 100 mM Tris-HCl, pH 8.5; SeMet-labeled *B. subtilis* SmcHead–$ScpA^N$-His_6 (23 mg ml^{-1}) in 8% isopropanol, 20 mM magnesium chloride and 50 mM MES, pH 6.5, all using the sitting-drop vapor-diffusion technique at 18 °C or 22 °C. X-ray diffraction data were collected at beamline BL41XU at the SPring-8 (Japan), beamline 5C at the Pohang Accelerator Laboratory (Korea) or PX beamline X10SA at the Swiss Light Source (Switzerland). For each crystal, a single-wavelength anomalous dispersion (SAD) data set was collected at the peak wavelength and used for phase determination. Structure solution and refinement statistics for the three structures are summarized in **Table 1**.

Gel-filtration assay. Analytical gel filtration of proteins was performed on Tricorn 10/300 GL columns prepacked with Superdex 200 or Superose 6 (GE Healthcare). Columns were equilibrated in 25 mM Tris (pH 7.4, 4 °C) and 200 mM NaCl, and ~1 mg of protein was injected in a sample volume of 700 µl. Fractions were precipitated with trichloroacetic acid (TCA) and sodium deoxycholate and resolved by SDS-PAGE.

***In vivo* cysteine cross-linking.** Cross-linking experiments were performed in LB if none of the strains showed a prokaryotic condensin phenotype. For experiments involving at least one nonfunctional condensin mutant, cells were grown in competence medium. Bacteria were allowed to grow to midexponential phase (OD_{600} of 0.4 in LB or OD_{600} of 0.05 in competence medium), then mixed with ~30% (w/v) ice, harvested by centrifugation and washed in ice-cold PBS with 0.1% glycerol (PBSG). Cells were resuspended in PBSG and the thiol-reactive cross-linker bismaleimidoethane (BMOE, Applichem) was added to a final concentration of 0.5 mM from a 20 mM stock in DMSO. When no cross-linker was used, an equal amount of DMSO was added. Cells were incubated for 10 min on ice, and the reaction was quenched by addition of 2-mercaptoethanol (2-ME) to a final concentration of 14 mM. Protein extracts were prepared by addition of TCA to a final concentration of 10% (w/v), followed by mechanical cell lysis and collection of precipitated protein by centrifugation.

HaloTag labeling and quantification of cross-linked species. Strains containing *smc* alleles bearing the HaloTag construct were grown and cross-linked with BMOE in triplicate as described above, except that cross-linking was performed in the presence of protease inhibitors (Sigma) and benzonase (Sigma). Following quenching with 2-ME, native extracts were prepared by incubation for 15 min at 37 °C with Ready-Lyse lysozyme solution (Epicentre) in the presence of 5 µM HaloTag TMR substrate (Promega). Proteins were separated by SDS-PAGE, and gels were scanned on a Typhoon scanner (GE Healthcare) with Cy3 DIGE filter setup. Band intensities were background corrected and quantified with ImageJ[46].

Viability assays. Cells were grown to stationary phase in liquid SMG, and dilutions were spotted onto NA or SMG agar plates. High-density spots contained about 7,000 cells (5 µl of 81-fold-diluted overnight culture) and low-density spots about 10 cells (5 µl of 59,049-fold-diluted culture). Plates were incubated at 37 °C for ~12 h on NA or ~36 h on SMG agar.

Nucleotide-mediated SmcHead engagement reaction. Purified PfSmcHead–ScpA and PfSmcHead–$ScpA^C$ complexes (100 µM) or a mixture of PfSmcHead and MBP-$PfScpA^C$ (100 µM each) were incubated with 2 mM or 10 mM AMP-PNP (Sigma) in a buffer containing 100 mM NaCl, 10 mM $MgCl_2$ and 20 mM Tris-HCl (pH 7.5) at 37 °C. Reaction mixtures were separated on a native gel and stained with Coomassie brilliant blue.

Antibodies. Monoclonal antibodies against the Pk and HA epitopes, clones SV5-Pk1 (AbD Serotec) and 12CA5 (Roche), respectively, were diluted 1:1,000 for immunoblotting. Rabbit polyclonal sera raised against *B. subtilis* DnaA[47] and Smc-His_6 protein (this paper) were used for immunoblotting at dilutions of 1:1,000 and 1:5,000, respectively.

44. Hamoen, L.W., Smits, W.K., de Jong, A., Holsappel, S. & Kuipers, O.P. Improving the predictive value of the competence transcription factor (ComK) binding site in *Bacillus subtilis* using a genomic approach. *Nucleic Acids Res.* **30**, 5517–5528 (2002).
45. Engler, C., Kandzia, R. & Marillonnet, S. A one pot, one step, precision cloning method with high throughput capability. *PLoS ONE* **3**, e3647 (2008).
46. Schneider, C.A., Rasband, W.S. & Eliceiri, K.W. NIH Image to ImageJ: 25 years of image analysis. *Nat. Methods* **9**, 671–675 (2012).
47. Scholefield, G., Errington, J. & Murray, H. Soj/ParA stalls DNA replication by inhibiting helix formation of the initiator protein DnaA. *EMBO J.* **31**, 1542–1555 (2012).

doi:10.1038/nsmb.2488

An asymmetric SMC–kleisin bridge in prokaryotic condensin

Frank Bürmann[1,5], Ho-Chul Shin[2,5], Jerome Basquin[3,5], Young-Min Soh[2], Victor Gimenez-Oya[1], Yeon-Gil Kim[4], Byung-Ha Oh[2] and Stephan Gruber[1]

[1]Max Planck Research Group “Chromosome Organization and Dynamics”, Max Planck Institute of Biochemistry, Martinsried, Germany. [2]KAIST Institute for the Biocentury, Department of Biological Sciences, Korea Advanced Institute of Science and Technology, Daejeon, Korea. [3]Department of Structural Cell Biology, Max Planck Institute of Biochemistry, Martinsried, Germany. [4]Pohang Accelerator Laboratory, Pohang University of Science and Technology, Pohang, Korea. [5]These authors contributed equally. Correspondence should be addressed to B.-H.O (bhoh@kaist.ac.kr) and S.G. (sgruber@biochem.mpg.de).

Nature Structural & Molecular Biology: doi:10.1038/nsmb.2488

Supplementary figures

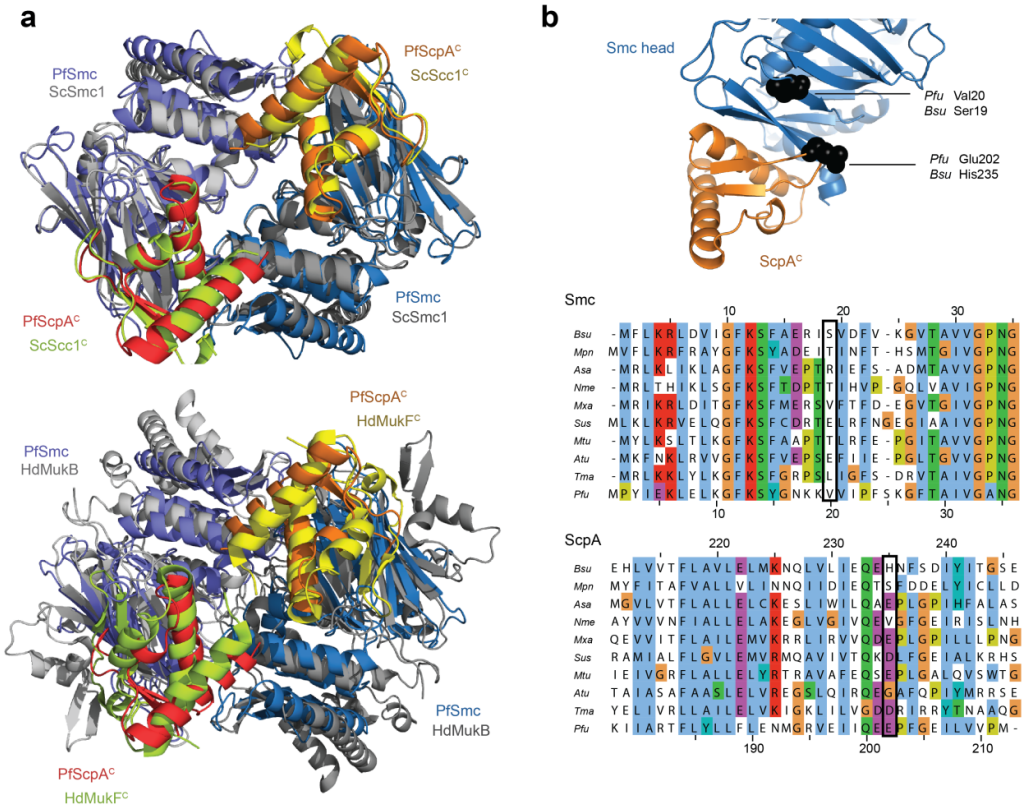

Supplementary Figure 1 The Smc–ScpA^C interface is conserved.
(**a**) Superimposition of the *P. furiosus* Smc–ScpA^C interface with the *S. cerevisiae* Smc1–Scc1^C interface (top panel, PDB: 1W1W) and the *Haemophilus ducreyi* MukB–MukF^C interface (bottom panel, PDB: 3EUJ). (**b**) Design of cross-linking mutants at the cap interface. Residues of *B. subtilis* Smc–ScpA that can be cross-linked by BMOE when mutated to cysteine are mapped onto the *P. furiosus* Smc–ScpA^C structure based on sequence alignments shown below. Chosen residues are highlighted with black boxes in the alignments. *Bsu*, *Bacillus subtilis*; *Mpn*, *Mycoplasma pneumoniae*; *Asa*, *Aeromonas salmonicidae*; *Nme*, *Neisseria meningitidis*; *Mxa*, *Myxococcus xhanthus*; *Sus*, *Solibacter usitatus*; *Mtu*, *Mycobacterium tuberculosis*; *Atu*, *Agrobacterium tumefaciens*; *Tma*, *Thermotoga maritima*; *Pfu*, *Pyrococcus furiosus*.

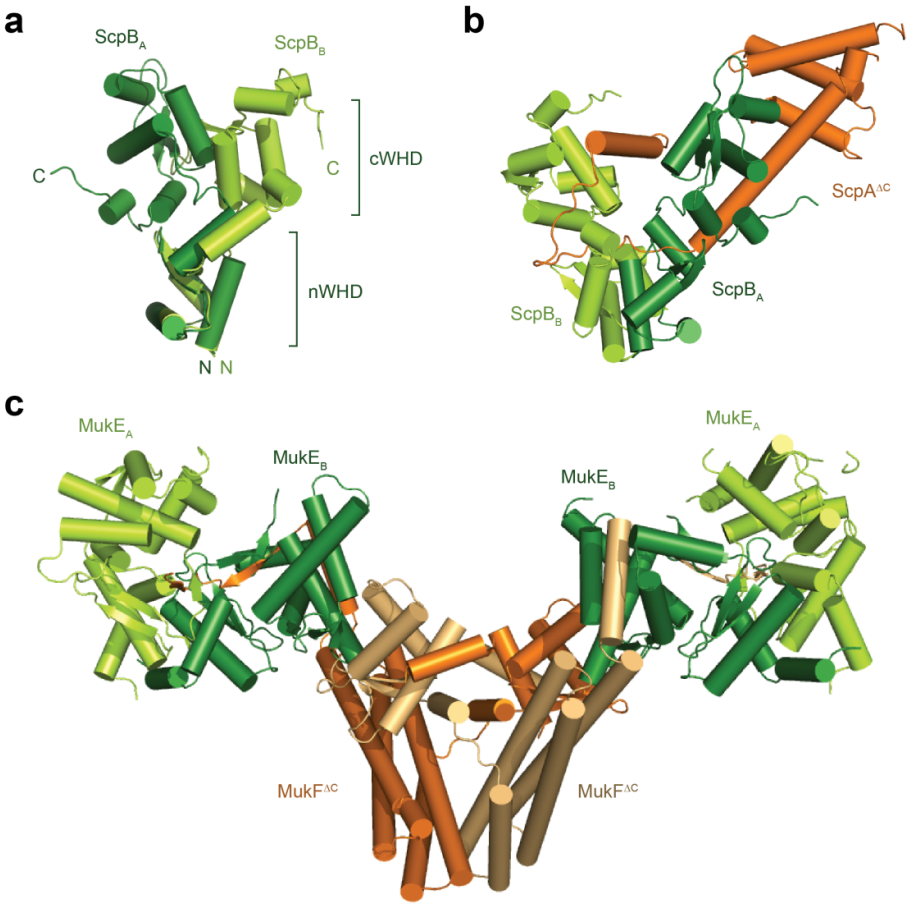

Supplementary Figure 2 Comparison of ScpAB and MukEF structures.
(**a**) Superimposition of both copies of ScpB observed in the ScpA$^{\Delta C}$–ScpB structure. N-terminal WHDs are aligned. (**b**) Structure of the ScpA$^{\Delta C}$–ScpB complex from *S. pneumoniae* as in **Fig. 2b**. ScpA and ScpB features are shown in orange and green colors, respectively. (**c**) Structure of the MukE–MukF$^{\Delta C}$ complex from *E. coli* (PDB: 3EUH). MukE and MukF features are displayed in green and orange colors, respectively.

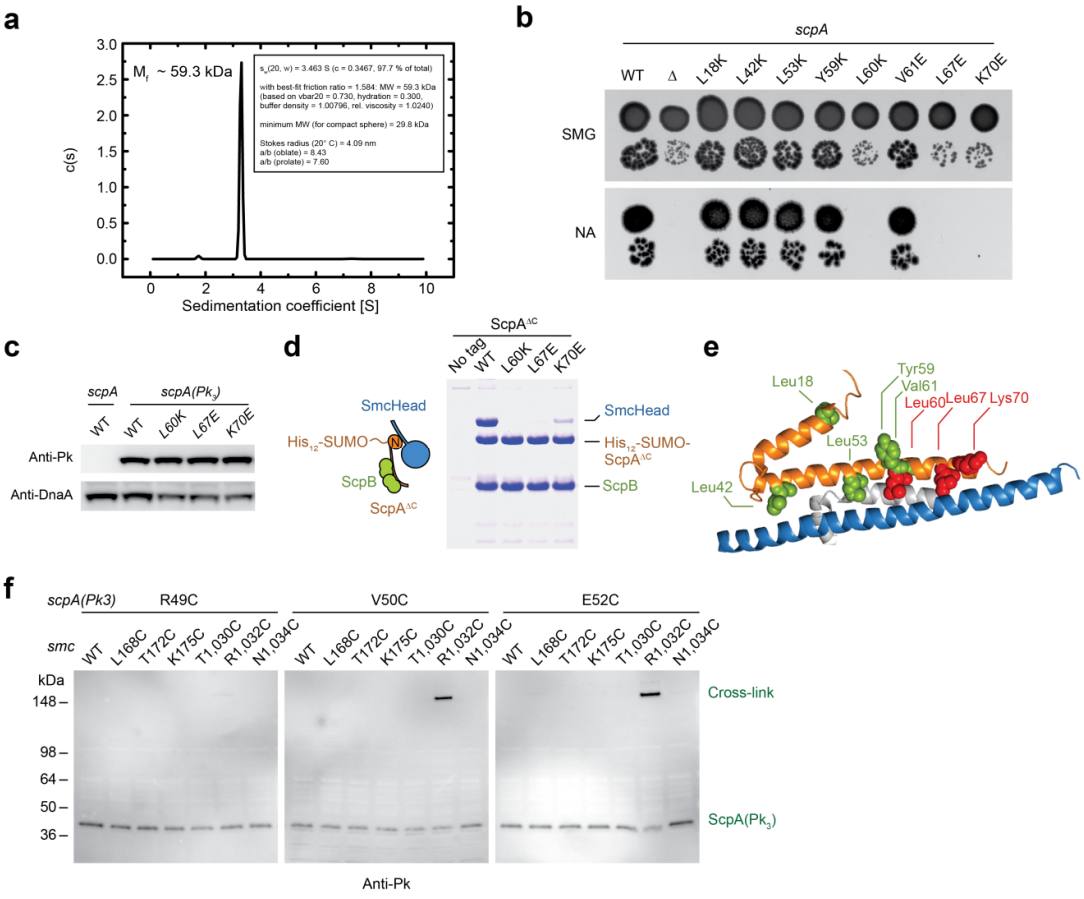

Supplementary Figure 3 Biochemical and genetic analysis of the Smc–ScpA^N interaction.
(**a**) *B. subtilis* SmcHead–ScpA^N-His$_6$ complexes are monomeric in solution. The distribution of sedimentation coefficients of SmcHead–ScpA^N-His$_6$ at 130 μM was determined by analytical ultracentrifugation. The best fit molecular weight (59.3 kDa) closely resembles the molecular weight of a monomeric complex (59.5 kDa). (**b**) Effects of mutations in the N-terminus of ScpA on colony formation. Strains BSG84, BSG397, BSG405, BSG407, BSG795 and BSG797-BSG801 were grown on minimal and rich medium (SMG and NA, respectively). (**c**) Cellular levels of mutated ScpA proteins. Extracts from strains BSG84, BSG165 and BSG804-806 were examined by blotting using antibodies against the Pk-tag and antiserum against DnaA. (**d**) Mutations in ScpA^N block interaction with Smc heads. *B. subtilis* SmcHead and ScpB proteins were co-expressed with wild-type and mutant ScpA^{ΔC} and purified via the His$_{12}$-SUMO-tag on ScpA^{ΔC}. Eluate fractions were analyzed by SDS-PAGE and Coomassie staining. (**e**) Mutated residues in ScpA generating wild-type and null-mutant phenotypes are shown in green and red colors, respectively. (**f**) A screen for juxtaposed residues at the Smc–ScpA^N interface. Same as in **Fig. 3d** showing full blots.

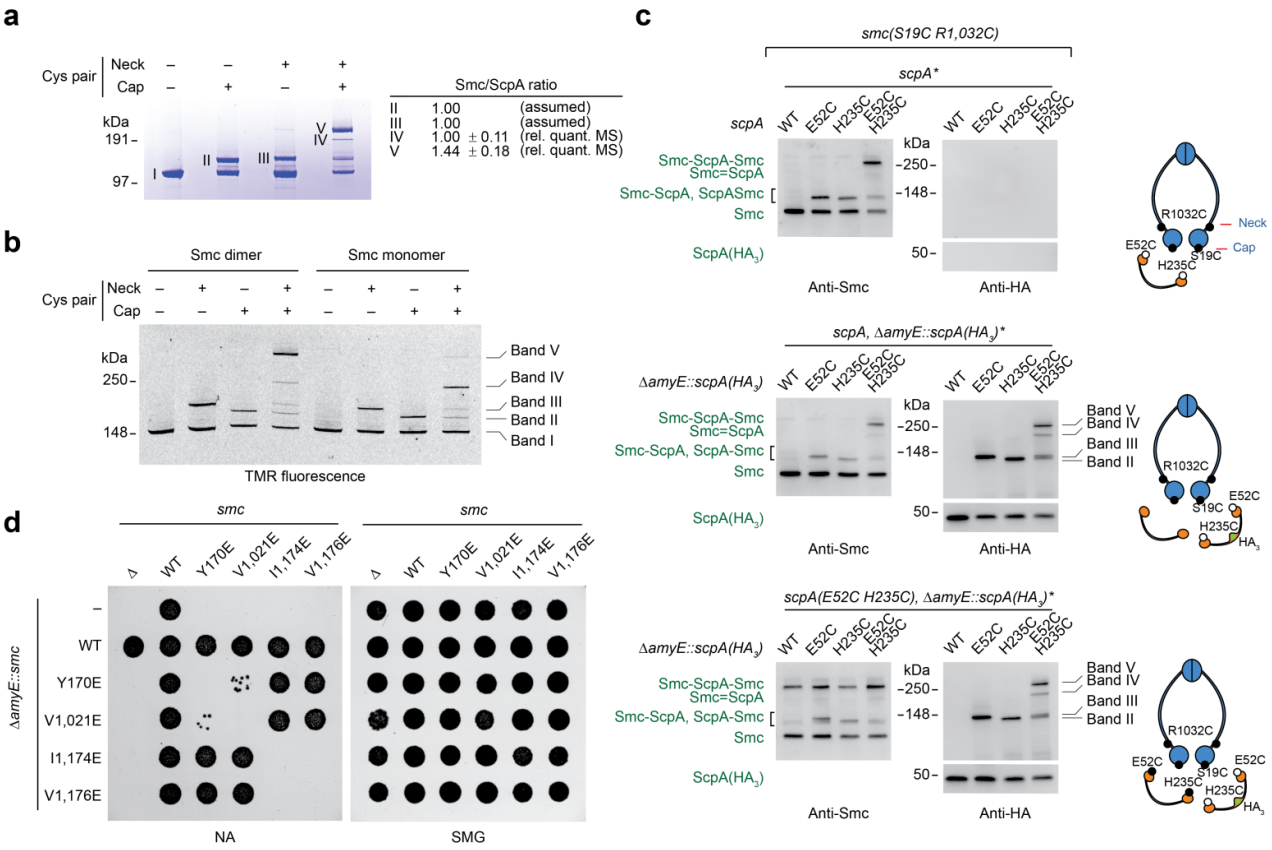

Supplementary Figure 4 Analysis of Smc–ScpA interactions *in vivo.*

(**a**) Mass-spectrometric analysis of cross-linked products isolated from *B. subtilis.* Strains BSG296 and BSG930-932 were cross-linked at the indicated interfaces with BMOE and complexes were affinity purified via a His_{12}-tag on Smc. Samples were resolved by SDS-PAGE (left panel) and the Smc/ScpA ratio of species was estimated by mass-spectrometry with relative quantification against peptides derived from single cross-link products (right panel). Purifications from all strains were performed in triplicate and peptide intensities from bands IV and V were compared to intensities from bands II and III within the replicates. Values are means ± s.d. combined from all replicates. (**b**) Smc dimerization at the hinge affects complex assembly. Smc(S19C R1,032C)-HaloTag and Smc(S19C G657A G658A G662A G663A R1,032C)-HaloTag deficient in dimerization were analyzed. Strains BSG689, BSG728-730 and BSG1292-1295 were grown in competence medium and cross-linked *in vivo* as in **Fig. 4c**. Halo-tagged Smc proteins were labeled by TMR in extracts and detected by in-gel fluorescence. (**c**) Smc dimers interact with only a single ScpA subunit in *B. subtilis*. Strains BSG536, BSG568, BSG609, BSG610 (top panel), BSG645-648 (middle panel) and BSG649-BSG652 (bottom panel) were cross-linked with BMOE. Protein extracts were analyzed by immunoblotting using Smc antiserum (left images) and antibodies against the HA epitope (right images). Experimental concepts: We directly tested whether the observed cross-linking species lacked a second copy of ScpA, as would be expected for Smc-ScpA-Smc and Smc=ScpA products. We generated strains that contain the Smc(S19C R1,032C) protein harboring acceptor cysteines at both interfaces and a ScpA allele that cross-links either to none (WT), one (E52C or H235C) or both (E52C H235C) of these sites. We then inserted into these strains an extra copy of ScpA that is internally tagged with three HA epitopes so that it can be distinguished from endogenous ScpA by immunoblotting. (Top panel) Strains lacking the ScpA(HA_3) extra copy displayed the expected cross-linking profile. (Middle panel) Likewise, ScpA(HA_3) with one or two cysteines produced a cross-linking pattern similar to endogenous, untagged ScpA when expressed in addition to endogenous wild-type ScpA. (Bottom panel) Crucially, in the presence of ScpA(E52C H235C), ScpA(HA_3) featuring either the E52C or the H235C mutation was never detected in the high molecular weight bands. (**d**) Mutual complementation of cap and neck mutants. Cells were spotted on NA or SMG and incubated at 37° C. The left panel is identical to **Fig. 4d**. Strains used: BSG2, BSG68, BSG508, BSG511, BSG697, BSG699-701, BSG703, BSG704, BSG720-725, BSG731, BSG732, BSG741-758.

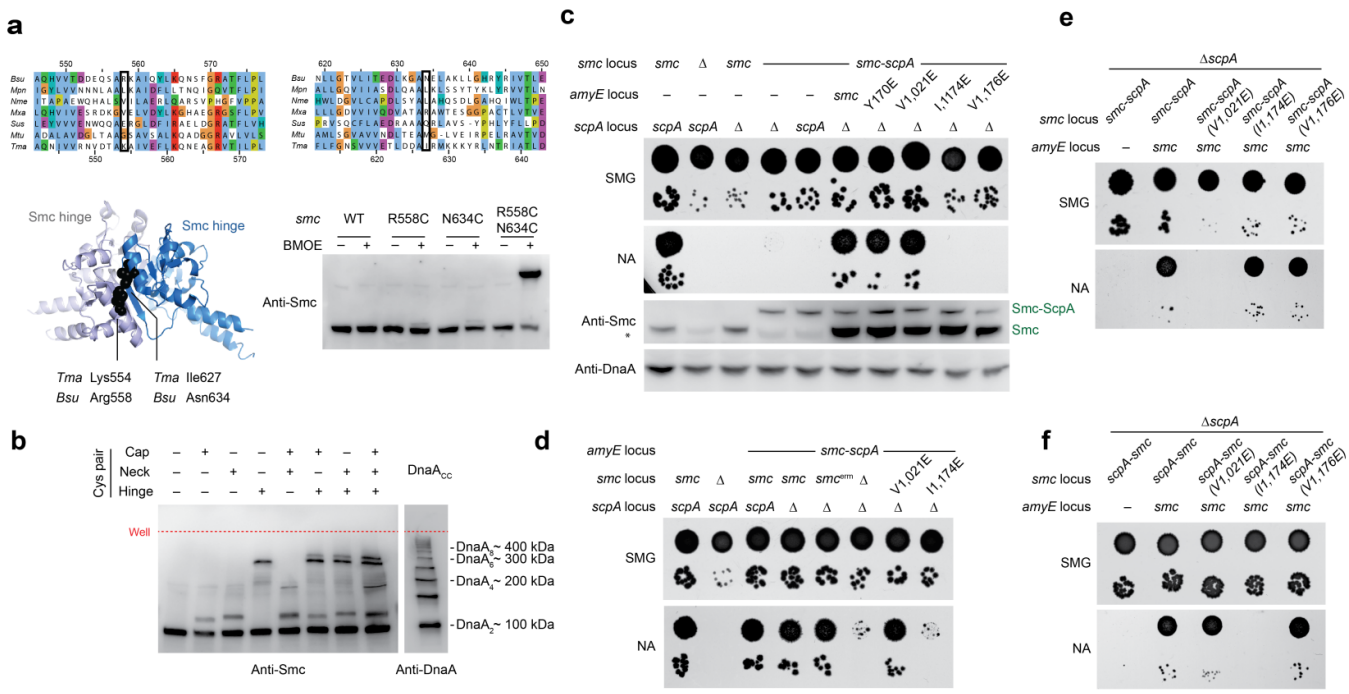

Supplementary Figure 5 Formation of covalent condensin rings and genetic analysis of Smc-ScpA fusions.

(**a**) Design of cross-linking mutants at the hinge interface of Smc. Based on sequence alignments (top) residues of *B. subtilis* Smc that can be cross-linked by BMOE when mutated to cysteine are mapped onto a *T. maritima* Smc hinge dimer structure (PDB: 1GXL, bottom left). Chosen residues are highlighted with black boxes in the alignments. Strains BSG2, BSG357, BSG828, BSG829 were cross-linked with BMOE and analyzed by immunoblotting as in **Fig. 1e** (bottom right). *Bsu*, *Bacillus subtilis*; *Mpn*, *Mycoplasma pneumoniae*; *Nme*, *Neisseria meningitidis*; *Mxa*, *Myxococcus xhanthus*; *Sus*, *Solibacter usitatus*; *Mtu*, *Mycobacterium tuberculosis*; *Tma*, *Thermotoga maritima*. (**b**) Absence of Smc–ScpA chains in untagged *B. subtilis* strains. Strains BSG1, BSG357, BSG372, BSG567, BSG568, BSG681, BSG692 and BSG693 were treated with BMOE and analyzed with antiserum against Smc. As control for transfer of high molecular weight species, BMOE cross-linked DnaA oligomers containing engineered cysteine residues were analyzed on the same membrane with antiserum against DnaA[1]. (**c**) Immunoblot analysis of strains used in **Fig. 5b** (bottom left panel) with antisera against Smc or DnaA (bottom panels). For clarity and direct comparison, data from **Fig. 5b** (bottom left panels) is also shown. (**d**) Strains expressing *Smc-ScpA* from an ectopic locus are rescued by Smc proteins expressed from the endogenous locus. Strains BSG2, BSG68, BSG901-905 and BSG907 were spotted on SMG or NA plates and incubated at 37° C. (**e**) Incorporation of the V1,021E neck mutation into Smc-ScpA fusion proteins is lethal on rich medium. Strains BSG398, BSG708, BSG934, BSG936 and BSG938 were grown on SMG and NA plates at 37° C. (**f**) V1,176E and I1,174E cap mutations in the ScpA-Smc fusion protein have no or strongly deteriorating effects on its functionality, respectively. Strains BSG1039, BSG1042, BSG1288-1290 were grown on SMG and NA agar plates at 37° C.

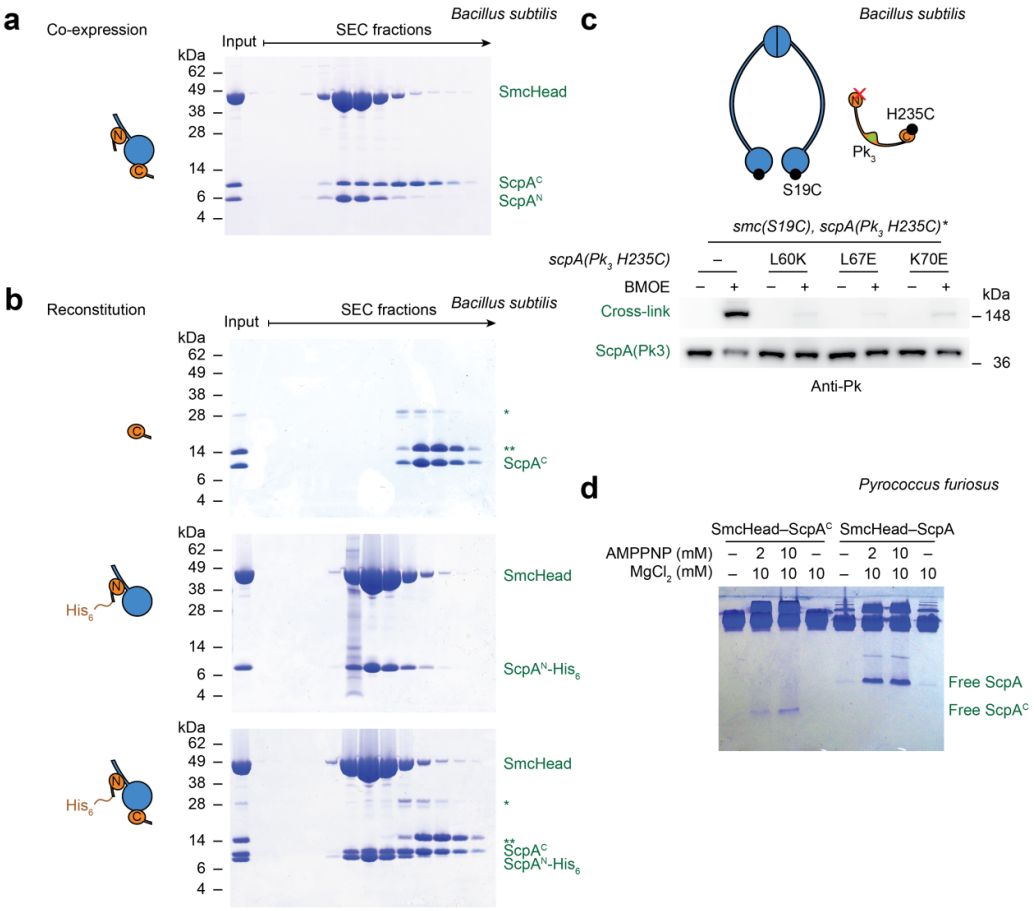

Supplementary Figure 6 Analysis of mechanisms promoting asymmetric complex assembly.
(**a**,**b**) Recombinant *Bacillus subtilis* ScpA^N and ScpA^C fragments can associate with the same SmcHead. *B. subtilis* SmcHead, ScpA^N and His$_6$-SUMO3-ScpA^C were co-expressed in *E. coli* and co-purified as a complex. After removal of the His$_6$-SUMO3-tag, complexes were run on Superdex 200 and fractions were analyzed by SDS-PAGE and Coomassie Blue staining (**a**). *B. subtilis* His$_6$-SUMO3-ScpA^C (*) was expressed in *E. coli* and purified. Its SenP2 cleavage products, His$_6$-SUMO3 (**) and ScpA^C, and purified SmcHead–ScpA^N-His$_6$ complexes were analyzed by SEC on Superdex 200. Fractions were examined by SDS-PAGE and Coomassie staining (**b**, top and middle panel). Similarly, a stoichiometric mixture of these proteins was fractionated by SEC (**b**, bottom panel).
(**c**) Mutations in ScpA's nαHD disrupt binding of the cWHD to Smc *in vivo*. Strains BSG917-920 were grown in minimal medium and incubated with either DMSO alone (–) or BMOE (+). Extracts were analyzed using Pk antibodies. (**d**) Dimerized *P. furiosus* Smc heads expel ScpA's cWHD *in vitro*. SmcHead (lacking the neck region) was incubated with ScpA^C or full-length ScpA in the presence of the non-hydrolysable ATP analogue AMPPNP and–or magnesium. Reactions were analyzed by native PAGE.

Supplementary Table 1 Cross-linking efficiency of ScpA–Smc cysteine pairs in *B. subtilis*.

	smc allele		
scpA allele	no cross-linking	weak or very weak cross-linking	substantial cross-linking
E3C	WT; K175C; T1,012C	L168C; T172C; E1,013C; T1,017C	–
Q5C	WT; K175C	L168C; T172C; T1,012C; E1,013C; T1,017C	–
K7C	WT; T1012C	L168C; T172C; K175C; E1,013C; T1,017C	–
D9C	WT; L168C; T172C; K175C; T1,012C; E1,013C	T1,017C	–
I8C	–	WT; L168C; T172C; K175C; T1,012C; E1,013C; T1,017C	–
T10C	WT; L168C; T172C; K175C; T1,012C; E1,013C	T1,017C	–
R49C	WT; L168C; T172C; K175C; T1,030C; N1,034C	R1,032C	–
V50C	WT; L168C; T172C; K175C; T1,030C; N1,034C	–	R1,032C
E52C	WT; T172C; K175C; T1,030C	L168C; N1,034C	R1,032C

Supplementary Table 2 List of *B. subtilis* strains and genotypes.

Strains are derived from *Bacillus subtilis* 168 ED[2] or *Bacillus subtilis* 168 1A700 (Bacillus Genetic Stock Centre).

Name	Genotype
BSG001	Bacillus subtilis 168 ED, trpC2 (see Domínguez-Cuevas P et al, Mol Micro 2012)
BSG002	168 ED, smc ftsY::ermB, trpC2
BSG003	168 ED, smc ftsY::specR, trpC2
BSG068	168 ED, Δsmc ftsY::ermB, trpC2
BSG084	168 ED, specR::scpA scpB, trpC2
BSG165	168 ED, specR::scpA(Pk3) scpB, trpC2
BSG296	168 ED, smc-His12::ermB, trpC2
BSG357	168 ED, smc(R558C, N634C) ftsY::specR, trpC2
BSG360	168 ED, smc(S19C) ftsY::ermB, trpC2
BSG367	168 ED, specR::scpA(H235C)scpB, trpC2
BSG372	168 ED, smc(S19C) ftsY::ermB, specR::scpA(H235C), trpC2
BSG396	168 ED, smc-CBP-scpA, ftsY::ermB, trpC2
BSG397	168 ED, specR::ΔscpA, scpB, trpC2
BSG398	168 ED, smc-CBP-scpA ftsY::ermB, specR::ΔscpA scpB, trpC2
BSG405	168 ED, specR::scpA(L42K) scpB, trpC2
BSG407	168 ED, specR::scpA(L18K) scpB, trpC2
BSG508	168 ED, smc(Y170E) ftsY::ermB, trpC2
BSG511	168 ED, smc(V1021E) ftsY::ermB, trpC2
BSG534	168 ED, specR::scpA(E52C, Pk3, H235C) scpB, trpC2
BSG536	168 ED, smc(S19C, R1032C) ftsY::ermB, trpC2
BSG567	168 ED, specR::scpA(E52C), smc(R1032C) ftsY::ermB, trpC2
BSG568	168 ED, specR::scpA(E52C, H235C), smc(S19C, R1032C) ftsY::ermB, trpC2
BSG609	168 ED, specR::scpA(E52C), smc(S19C, R1032C) ftsY::ermB, trpC2
BSG610	168 ED, specR::scpA(H235C), smc(S19C, R1032C) ftsY::ermB, trpC2
BSG645	168 ED, smc(S19C, R1032C) ftsY::ermB, ΔamyE::scpA(HA3)::CAT, trpC2
BSG646	168 ED, smc(S19C, R1032C) ftsY::ermB, ΔamyE::scpA(E52C, HA3)::CAT, trpC2
BSG647	168 ED, smc(S19C, R1032C) ftsY::ermB, ΔamyE::scpA(HA3, H235C)::CAT, trpC2
BSG648	168 ED, smc(S19C, R1032C) ftsY::ermB, ΔamyE::scpA(E52C, HA3, H235C)::CAT, trpC2
BSG649	168 ED, specR::scpA(E52C, H235C) scpB, smc(S19C, R1032C) ftsY::ermB, ΔamyE::scpA(HA3)::CAT, trpC2
BSG650	168 ED, specR::scpA(E52C, H235C) scpB, smc(S19C, R1032C) ftsY::ermB, ΔamyE::scpA(E52C, HA3)::CAT, trpC2
BSG651	168 ED, specR::scpA(E52C, H235C) scpB, smc(S19C, R1032C) ftsY::ermB, ΔamyE::scpA(HA3, H235C)::CAT, trpC2
BSG652	168 ED, specR::scpA(E52C, H235C) scpB, smc(S19C, R1032C) ftsY::ermB, ΔamyE::scpA(E52C, HA3, H235C)::CAT, trpC2
BSG681	168 ED, specR::scpA(E52C, H235C) scpB, smc(S19C, R558C, N634C, R1032C) ftsY::ermB, trpC2
BSG689	168 ED, smc(S19C, R1032C)-TEV-HaloTag ftsY::ermB, trpC2
BSG692	168 ED, specR::scpA(E52C) scpB, smc(S19C, R558C, N634C, R1032C) ftsY::ermB, trpC2
BSG693	168 ED, specR::scpA(H235C) scpB, smc(S19C, R558C, N634C, R1032C) ftsY::ermB, trpC2
BSG697	168 ED, smc ftsY::ermB, ΔamyE::smc::CAT, trpC2
BSG699	168 ED, smc ftsY::ermB, ΔamyE::smc(V1176E)::CAT, trpC2
BSG700	168 ED, smc ftsY::ermB, ΔamyE::smc(I1174E)::CAT, trpC2
BSG701	168 ED, Δsmc ftsY::ermB, ΔamyE::smc::CAT, trpC2
BSG703	168 ED, Δsmc ftsY::ermB, ΔamyE::smc(V1176E)::CAT, trpC2
BSG704	168 ED, Δsmc ftsY::ermB, ΔamyE::smc(I1174E)::CAT, trpC2
BSG708	168 ED, smc-CBP-scpA ftsY::ermB, specR::ΔscpA scpB, ΔamyE::smc::CAT, trpC2
BSG709	168 ED, smc-CBP-scpA ftsY::ermB, specR::ΔscpA scpB, ΔamyE::smc(V1176E)::CAT, trpC2
BSG710	168 ED, smc-CBP-scpA ftsY::ermB, specR::ΔscpA scpB, ΔamyE::smc(I1174E)::CAT, trpC2
BSG720	168 ED, smc(Y170E) ftsY::ermB, ΔamyE::smc::CAT, trpC2
BSG721	168 ED, smc(Y170E) ftsY::ermB, ΔamyE::smc(V1176E)::CAT, trpC2
BSG722	168 ED, smc(Y170E) ftsY::ermB, ΔamyE::smc(I1174E)::CAT, trpC2
BSG723	168 ED, smc(V1021E) ftsY::ermB, ΔamyE::smc::CAT, trpC2
BSG724	168 ED, smc(V1021E) ftsY::ermB, ΔamyE::smc(V1176E)::CAT, trpC2
BSG725	168 ED, smc(V1021E) ftsY::ermB, ΔamyE::smc(I1174E)::CAT, trpC2
BSG728	168 ED, specR::scpA(E52C), smc(S19C, R1032C)-TEV-HaloTag ftsY::ermB, trpC2
BSG729	168 ED, specR::scpA(H235C), smc(S19C, R1032C)-TEV-HaloTag ftsY::ermB, trpC
BSG730	168 ED, specR::scpA(E52C, H235C), smc(S19C, R1032C)-TEV-HaloTag ftsY::ermB, trpC2
BSG731	168 ED, smc(V1176E) ftsY::ermB, trpC2
BSG732	168 ED, smc(I1174E) ftsY::ermB, trpC2
BSG737	168 ED, smc-CBP-scpA ftsY::ermB, specR::ΔscpA scpB, ΔamyE::smc(Y170E)::CAT, trpC2
BSG738	168 ED, smc-CBP-scpA ftsY::ermB, specR::ΔscpA scpB, ΔamyE::smc(V1021E)::CAT, trpC2
BSG741	168 ED, smc(V1176E) ftsY::ermB, ΔamyE::smc::CAT, trpC2
BSG742	168 ED, smc(V1176E) ftsY::ermB, ΔamyE::smc(V1176E)::CAT, trpC2
BSG743	168 ED, smc(V1176E) ftsY::ermB, ΔamyE::smc(I1174E)::CAT, trpC2
BSG744	168 ED, smc(I1174E) ftsY::ermB, ΔamyE::smc::CAT, trpC2
BSG745	168 ED, smc(I1174E) ftsY::ermB, ΔamyE::smc(V1176E)::CAT, trpC2
BSG746	168 ED, smc(I1174E) ftsY::ermB, ΔamyE::smc(I1174E)::CAT, trpC2

Name	Genotype
BSG747	168 ED, smc ftsY::ermB, ΔamyE::smc(Y170E)::CAT, trpC2
BSG748	168 ED, smc ftsY::ermB, ΔamyE::smc(V1021E)::CAT, trpC2
BSG749	168 ED, Δsmc ftsY::ermB, ΔamyE::smc(Y170E)::CAT, trpC2
BSG750	168 ED, Δsmc ftsY::ermB, ΔamyE::smc(V1021E)::CAT, trpC2
BSG751	168 ED, smc(Y170E) ftsY::ermB, ΔamyE::smc(Y170E)::CAT, trpC2
BSG752	168 ED, smc(Y170E) ftsY::ermB, ΔamyE::smc(V1021E)::CAT, trpC2
BSG753	168 ED, smc(V1021E) ftsY::ermB, ΔamyE::smc(Y170E)::CAT, trpC2
BSG754	168 ED, smc(V1021E) ftsY::ermB, ΔamyE::smc(V1021E)::CAT, trpC2
BSG755	168 ED, smc(V1176E) ftsY::ermB, ΔamyE::smc(Y170E)::CAT, trpC2
BSG756	168 ED, smc(V1176E) ftsY::ermB, ΔamyE::smc(V1021E)::CAT, trpC2
BSG757	168 ED, smc(I1174E) ftsY::ermB, ΔamyE::smc(Y170E)::CAT, trpC2
BSG758	168 ED, smc(I1174E) ftsY::ermB, ΔamyE::smc(V1021E)::CAT, trpC2
BSG768	168 ED, specR::scpA ΔscpB, trpC2
BSG795	168 ED, specR::scpA(L53K) scpB, trpC+
BSG797	168 ED, specR::scpA(Y59K) scpB, trpC+
BSG798	168 ED, specR::scpA(L60K) scpB, trpC+
BSG799	168 ED, specR::scpA(V61E) scpB, trpC+
BSG800	168 ED, specR::scpA(L67E) scpB, trpC+
BSG801	168 ED, specR::scpA(K70E) scpB, trpC+
BSG804	168 ED, specR::scpA(L60K, Pk3) scpB, trpC+
BSG805	168 ED, specR::scpA(L67E, Pk3) scpB, trpC+
BSG806	168 ED, specR::scpA(K70E, Pk3) scpB, trpC+
BSG828	168 ED, smc(R558C) ftsY::specR, trpC2
BSG829	168 ED, smc(N634C) ftsY::specR, trpC2
BSG859	168 ED, smc(S19C) ftsY::ermB, specR::scpA(E52C, Pk3, H235C) scpB, trpC2
BSG860	168 ED, smc(S19C, Y170E) ftsY::ermB, specR::scpA(E52C, Pk3, H235C) scpB, trpC2
BSG861	168 ED, smc(S19C, V1021E) ftsY::ermB, specR::scpA(E52C, Pk3, H235C) scpB, trpC2
BSG862	168 ED, smc(R1032C) ftsY::ermB, specR::scpA(E52C, Pk3, H235C) scpB, trpC2
BSG863	168 ED, smc(R1032C, I1774E) ftsY::ermB, specR::scpA(E52C, Pk3, H235C) scpB, trpC2
BSG864	168 ED, smc(R1032C, I1776E) ftsY::ermB, specR::scpA(E52C, Pk3, H235C) scpB, trpC2
BSG866	168 ED, smc(S19C) ftsY::ermB, specR::scpA(H235C) ΔscpB, trpC2
BSG868	168 ED, smc(R1032C) ftsY::ermB, specR::scpA(E52C) ΔscpB, trpC2
BSG901	168 ED, ΔamyE::smc-CBP-scpA::CAT, trpC2
BSG902	168 ED, ΔamyE::smc-CBP-scpA::CAT, specR::ΔscpA scpB, trpC2
BSG903	168 ED, ΔamyE::smc-CBP-scpA::CAT, specR::ΔscpA scpB, smc ftsY::ermB, trpC2
BSG904	168 ED, ΔamyE::smc-CBP-scpA::CAT, specR::ΔscpA scpB, Δsmc ftsY::ermB, trpC2
BSG905	168 ED, ΔamyE::smc-CBP-scpA::CAT, specR::ΔscpA scpB, smc(V1021E) ftsY::ermB, trpC2
BSG907	168 ED, ΔamyE::smc-CBP-scpA::CAT, specR::ΔscpA scpB, smc(I1174E) ftsY::ermB, trpC2
BSG917	168 ED, smc(S19C) ftsY::ermB, specR::scpA(Pk3, H235C) scpB, trpC2
BSG918	168 ED, smc(S19C) ftsY::ermB, specR::scpA(L60K, Pk3, H235C) scpB, trpC2
BSG919	168 ED, smc(S19C) ftsY::ermB, specR::scpA(L67E, Pk3, H235C) scpB, trpC2
BSG920	168 ED, smc(S19C) ftsY::ermB, specR::scpA(K70E, Pk3, H235C) scpB, trpC2
BSG929	168 ED, smc(S19C, R1032C) ftsY::ermB, specR::scpA(E52C, H235C) ΔscpB, trpC2
BSG930	168 ED, smc(S19C)-His12 ftsY::ermB, specR::scpA(H235C), lysA*, trpC+
BSG931	168 ED, smc(R1032C)-His12 ftsY::ermB, specR::scpA(E52C), lysA*, trpC+
BSG932	168 ED, specR::scpA(E52C, H235C), smc(S19C, R1032C)-His12 ftsY::ermB, lysA*, trpC+
BSG934	168 ED, smc(V1021E)-CBP-scpA ftsY::ermB, specR::ΔscpA scpB, ΔamyE::smc::CAT, trpC2
BSG937	168 ED, smc(I1174E)-CBP-scpA ftsY::ermB, specR::ΔscpA scpB, ΔamyE::smc::CAT, trpC2
BSG940	168 ED, smc(V1176E)-CBP-scpA ftsY::ermB, specR::ΔscpA scpB, ΔamyE::smc::CAT, trpC2
BSG953	168 ED, smc(S19C, K37I, R1032C) ftsY::ermB, specR::scpA(E52C, H235C), ΔamyE::scpA(HA3)::CAT, trpC2
BSG954	168 ED, smc(S19C, K37I, R1032C) ftsY::ermB, specR::scpA(E52C, H235C), ΔamyE::scpA(E52C, HA3)::CAT, trpC2
BSG955	168 ED, smc(S19C, K37I, R1032C) ftsY::ermB, specR::scpA(E52C, H235C), ΔamyE::scpA(HA3, H235C)::CAT, trpC2
BSG956	168 ED, smc(S19C, K37I, R1032C) ftsY::ermB, specR::scpA(E52C, H235C), ΔamyE::scpA(E52C, HA3, H235C)::CAT, trpC2
BSG957	168 ED, smc(S19C, R1032C, S1090R) ftsY::ermB, specR::scpA(E52C, H235C), ΔamyE::scpA(HA3)::CAT, trpC2
BSG958	168 ED, smc(S19C, R1032C, S1090R) ftsY::ermB, specR::scpA(E52C, H235C), ΔamyE::scpA(E52C, HA3)::CAT, trpC2
BSG959	168 ED, smc(S19C, R1032C, S1090R) ftsY::ermB, specR::scpA(E52C, H235C), ΔamyE::scpA(HA3, H235C)::CAT, trpC2
BSG960	168 ED, smc(S19C, R1032C, S1090R) ftsY::ermB, specR::scpA(E52C, H235C), ΔamyE::scpA(E52C, HA3, H235C)::CAT, trpC2
BSG961	168 ED, smc(S19C, R1032C, D1117A) ftsY::ermB, specR::scpA(E52C, H235C), ΔamyE::scpA(HA3)::CAT, trpC2
BSG962	168 ED, smc(S19C, R1032C, D1117A) ftsY::ermB, specR::scpA(E52C, H235C), ΔamyE::scpA(E52C, HA3)::CAT, trpC2
BSG963	168 ED, smc(S19C, R1032C, D1117A) ftsY::ermB, specR::scpA(E52C, H235C), ΔamyE::scpA(HA3, H235C)::CAT, trpC2
BSG964	168 ED, smc(S19C, R1032C, D1117A) ftsY::ermB, specR::scpA(E52C, H235C), ΔamyE::scpA(E52C, HA3, H235C)::CAT, trpC2
BSG965	168 ED, smc(S19C, R1032C, E1118Q) ftsY::ermB, specR::scpA(E52C, H235C), ΔamyE::scpA(HA3)::CAT, trpC2
BSG966	168 ED, smc(S19C, R1032C, E1118Q) ftsY::ermB, specR::scpA(E52C, H235C), ΔamyE::scpA(E52C, HA3)::CAT, trpC2
BSG967	168 ED, smc(S19C, R1032C, E1118Q) ftsY::ermB, specR::scpA(E52C, H235C), ΔamyE::scpA(HA3, H235C)::CAT, trpC2
BSG968	168 ED, smc(S19C, R1032C, E1118Q) ftsY::ermB, specR::scpA(E52C, H235C), ΔamyE::scpA(E52C, HA3, H235C)::CAT, trpC2
BSG969	168 ED, smc(S19C, R1032C) ftsY::ermB, specR::scpA(E52C, H235C) ΔscpB, ΔamyE::scpA(HA3)::CAT, trpC2
BSG970	168 ED, smc(S19C, R1032C) ftsY::ermB, specR::scpA(E52C, H235C) ΔscpB, ΔamyE::scpA(E52C, HA3)::CAT, trpC2
BSG971	168 ED, smc(S19C, R1032C) ftsY::ermB, specR::scpA(E52C, H235C) ΔscpB, ΔamyE::scpA(HA3, H235C)::CAT, trpC2
BSG972	168 ED, smc(S19C, R1032C) ftsY::ermB, specR::scpA(E52C, H235C) ΔscpB, ΔamyE::scpA(E52C, HA3, H235C)::CAT, trpC2
BSG1004	1A700, specR::ΔscpA scpB, trpC2
BSG1005	1A700, specR::scpA scpB, trpC2
BSG1039	1A700, rncS scpA-tevX3-smc ftsY::ermB, specR::ΔscpA scpB, trpC2
BSG1042	1A700, rncS scpA-tevX3-smc ftsY::ermB, specR::ΔscpA scpB, ΔamyE::smc::CAT, trpC2
BSG1043	1A700, rncS scpA-tevX3-smc ftsY::ermB, specR::ΔscpA scpB, ΔamyE::smc(V1021E)::CAT, trpC2
BSG1044	1A700, rncS scpA-tevX3-smc ftsY::ermB, specR::ΔscpA scpB, ΔamyE::smc(I1174E)::CAT,trpC2
BSG1077	168 ED, smc(S19C, R558C, N634C, R1032C)-TEV-HaloTag ftsY::ermB, trpC2

Name	Genotype
BSG1078	168 ED, smc(S19C, R558C, N634C, R1032C)-TEV-HaloTag ftsY::ermB, scpA(E52C, H235C), trpC2
BSG1288	1A700, rncS scpA-tevX3-smc(V1021E) ftsY::ermB, specR::ΔscpA scpB, ΔamyE::smc::CAT, trpC2
BSG1289	1A700, rncS scpA-tevX3-smc(I1174E) ftsY::ermB, specR::ΔscpA scpB, ΔamyE::smc::CAT, trpC2
BSG1290	1A700, rncS scpA-tevX3-smc(I1176E) ftsY::ermB, specR::ΔscpA scpB, ΔamyE::smc::CAT, trpC2
BSG1292	168 ED, smc(S19C, G657A, G658A, G662A, G663A, R1032C)-TEV-HaloTag ftsY::ermB, trpC2
BSG1293	168 ED, specR::scpA(E52C), smc(S19C, G657A, G658A, G662A, G663A, R1032C)-TEV-HaloTag ftsY::ermB, trpC2
BSG1294	168 ED, specR::scpA(H235C), smc(S19C, G657A, G658A, G662A, G663A, R1032C)-TEV-HaloTag ftsY::ermB, trpC2
BSG1295	168 ED, specR::scpA(E52C, H235C), smc(S19C, G657A, G658A, G662A, G663A, R1032C)-TEV-HaloTag ftsY::ermB, trpC2

Supplementary Table 3 List of recombinant protein constructs.

Originating species	Protein construct	Figure appearance
P. furiosus	(1-182-SGGSGGS-1,006-1,186)Smc	1b, 6b, S1ab, S6d
P, furiosus	(126-212)ScpA	1b, 4a, 7, S1
P. furiosus	His_{10}-MBP-NSSSNNNNNNNNNNLGLEENLYFQG-(126-212)ScpA	6b
S. pneumoniae	(1-160)$ScpA^{\Delta C}$	2b, 3f, 4a, 7
S. pneumoniae	(1-183)ScpB	2b, 4a, 7, S2
B. subtilis	Smc	3a
B. subtilis	Met-(161-219-GPG-983-1,037)Smc	3a
B. subtilis	(1-219-GPG-983-1,186)Smc	3a, 3f, S3d, S6ab
B. subtilis	(1-219-GPG-983-1,186)Smc-SR	1e, 3c, S3d
B. subtilis	(1-219-GPG-983-1,186)Smc-SRGNGSGH_{12}TR and mutants thereof	1e, 3c
B. subtilis	(1-86)ScpA	3c, S6a
B. subtilis	(1-86)ScpA-TSH_6	3aef, 4a, 7a, S3, S6b
B. subtilis	(1-168)ScpA	S3d
B. subtilis	His12-SUMO-(1-168)ScpA and mutants thereof	S3d
B. subtilis	Met-(148-251)ScpA	1e, S6ab
B. subtilis	ScpB	S3d

Supplementary Note

Purification of recombinant *B. subtilis* protein constructs and pull-down assays

Recombinant constructs of *B. subtilis* proteins were produced from pET-28 derived plasmids by Isopropyl-β-D-thio-galactoside (IPTG) induction or auto-induction in *E. coli* BL21-Gold (DE3) cells[3]. SmcHead constructs contained residues 1-219 and 983-1186 connected by a GPG linker. SmcHead-His_{12} constructs contained an additional C-terminal SRGNGSGHHHHHHHHHHHHTR peptide. $ScpA^N$ (residues 1-86) was expressed either untagged or with a C-terminal TSHHHHHH peptide. $ScpA^C$ (residues 148-251) was expressed either untagged or with an N-terminal His_6-SUMO3 tag. Protein extracts were prepared by mechanical grinding of frozen cell suspensions in 50 mM sodium phosphate buffer (pH 7.4, 4° C) with 300 mM NaCl, 10 % glycerol, benzonase, protease inhibitor cocktail (Sigma) and 40 mM imidazole for His_6-tagged constructs and 80 mM imidazole for His_{12}-tagged constructs, respectively. Cell debris was pelleted by centrifugation at 50,000 x g for 2 x 20 min. Initial purification was performed by passage over Ni Sepharose High Performance (GE Healthcare), extensive washing with binding buffer and gradient elution into 500 mM imidazole (pH 7.4, 4° C), 300 mM NaCl, 10 % glycerol. Protein complexes were further purified by gel filtration on Superdex 200 into 25 mM Tris (pH 7.4, 4° C), 200 mM NaCl. Reconstituted ternary complexes of SmcHead–$ScpA^N$-His_6–$ScpA^C$ were formed by mixing SmcHead–$ScpA^N$-His_6 complex with an equimolar amount of SenP2 protease cleaved His_6-SUMO3-$ScpA^C$, and incubation for 1 h on ice. Untagged ternary complex of SmcHead–$ScpA^N$–$ScpA^C$ was prepared by co-expression of SmcHead, $ScpA^N$ and His_6-SUMO3-$ScpA^C$, and purified as described above. The tag was removed by His_6-SenP2 digestion at 4° C, passage over Ni Sepharose FF (GE Healthcare) in the presence of 40 mM imidazole, and desalting on Sephadex G25 (GE Healthcare). Proteins were concentrated in Vivaspin 15 10k MWCO filters (Sartorius). Concentrations were determined by UV absorbance using theoretical extinction coefficients. Pull-down assays with *E. coli* extracts were performed similarly as described above using HisMag Sepharose particles (GE-Healthcare).

Production, crystallization and X-ray structure determination of BsSmcHead–$ScpA^N$-His_6

Selenomethionine (SelMet) labeled SmcHead–$ScpA^N$-His_6 was produced in BL21-Gold (DE3) by a methionine biosynthesis feedback inhibition protocol. The complex was purified as described above, except that all buffers contained 5 mM DTT. The protein was concentrated to 23 mg ml^{-1} and was crystallized in 8 % isopropanol, 20 mM magnesium chloride and 50 mM MES pH 6.5 using the sitting-drop vapor diffusion technique at 18° C. SmcHead–$ScpA^N$-His_6 crystals grew to about $0.3 \times 0.1 \times 0.1$ mm in size. Crystals were cryoprotected in mother liquor supplemented with 20 % glycerol, mounted in nylon loops and flash-frozen in liquid nitrogen for data collection at 100 K. X-ray diffraction data were collected at the PX beamline X10SA at the Swiss Light Source (Villigen, Switzerland) using a Pilatus 6M detector and processed with the program XDS[4]. We obtained phases from a SAD data set collected to 3.4 Å resolution with synchrotron radiation tuned at the peak wavelength of the selenium absorption edge. After substructure solution and phasing with Phenix AutoSol, an initial model was built automatically with BUCCANEER[5] and extended manually in Coot[6]. Structure refinement was carried out using Phenix.refine with TLS and twinning refinement[7].

Production, crystallization and X-ray structure determination of PfSmcHead–ScpA^{C}

Genomic DNA of *P. furiosus* DSM3638 was used as template for gene cloning. DNA fragments encoding the N- and C-terminal domains and a short coiled coil region (residues 1-182, and 1,006-1,177) were amplified by PCR and the two DNA fragments were connected by an artificial linker encoding a SGGSGGS sequence. The selected protein regions are identical to those for the structural study of free and nucleotide-bound SmcHead[8]. Using the *Nde*I–*Sal*I cloning sites, the resulting DNA was ligated into a pET22b-CPD 10H plasmid, an in-house modified form of the pET22b plasmid (Novagen) to express a protein fused to His_{10}-tagged CPD (cysteinyl protease domain) at the C-terminus[9]. A DNA fragment encoding the cWHD (residues 126-212; ScpA^{C}) was inserted into a 10H GST pProEx HTa vector using the *Nde*I–*Xho*I sites. This vector was generated by modifying the pProEx HTa vector (Invitrogen) to contains the glutathione-S-transferase (GST) gene with an N-terminal His_{10}-tag. SmcHead-CPD-His_{10} and His_{10}-GST-ScpA^{C} were individually expressed in the *E. coli* BL21 (DE3) RIPL strain (Stratagene) grown in LB medium at 18° C. Protein expression was induced by IPTG, when the OD_{600} reached 0.6. Bacterial lysates with overexpressed SmcHead-CPD-His_{10} and His_{10}-GST-ScpA^{C} were each prepared by sonication in Buffer A (20 mM Tris-HCl pH 7.5, 100 mM NaCl, and 1 mM NaN_3) containing 5 mM 2-mercaptoethanol (2-ME). The supernatants of each sample were applied to gravity flow columns filled with HisPur cobalt Resin (Thermo). The resin-bound SmcHead-CPD-His_{10} was treated with Buffer A containing 0.1 mM phytate to remove the CPD-His_{10} tag and the protein was eluted from the column with Buffer A. His_{10}-GST-ScpA^{C} was eluted with buffer A containing 150 mM imidazole and digested with TEV protease to remove the His_{10}-GST tag at the N-terminus of the protein. These samples were further purified with a HiTrap Q anion exchange column (GE Healthcare) and mixed together. This mixture was loaded on to HiLoad 26/60 Superdex 75 gel filtration column (GE Healthcare), equilibrated with Buffer A containing 1 mM DTT. Purified SmcHead–ScpA^{C} sample was concentrated to 10 mg ml^{-1} using Amicon Ultra 30K (Millipore). Selenomethionine substituted SmcHead (SelMet-SmcHead) was produced in the *E. coli* B834 (DE3) methionine auxotroph (Novagen), and partially purified as described above. This protein was used to produce the SmcHead–ScpA^{C} complex with SelMet substitution only in SmcHead. To obtain crystals of the complex, 576 different commercially available precipitant solutions were screened with the nanoliter pipetting system Mosquito (TTP Labtech) at 22° C. Initial crystals grew in a solution containing 200 mM ammonium phosphate dibasic and 20 % polyethylene glycol 3,350. Larger single crystals were obtained by hanging-drop vapor-diffusion method at 22° C from a precipitant solution containing 220 mM ammonium phosphate dibasic, 16 % polyethylene glycol 3,350 and 100 mM Bicine pH 9.0. A single-wavelength anomalous dispersion (SAD) data set was collected with a crystal of the complex of SelMet-SmcHead and ScpA^{C} at the beamline BL41XU at the SPring-8, Japan. Selenium positions were identified by the programs ShelxD[10] and used for phase determination by SHARP[11], followed by density modification by SOLOMON[12]. The program ARP/wARP[13] was used for automated model building, which yielded about 90 % of the complete model. Subsequently, manual model building was performed using Coot[6], and the structure was refined using CNS[14]. The final model does not include residues 170-182, 1,006, 1,162-1,177 and the artificial linker sequence of SmcHead and residues 126-142 of ScpA whose electron densities were missing or barely visible.

Production, crystallization and X-ray structure determination of SpScpA$^{\Delta C}$–ScpB

DNA fragments encoding the N-terminal 160 residues of ScpA (NP_359283; 242 residues) lacking cWHD and the N-terminal 183 residues of ScpB (NP_359282; 189 residues) of *S. pneumonia* R6 were amplified and ligated into a pCDFDuet CPD 10H vector derived from the pCDFDuet plasmid (Novagen), a construct to co-express ScpA$^{\Delta C}$ without a tag and ScpB-CPD-His_{10} in *E. coli*. ScpA$^{\Delta C}$ and ScpB-CPD-His_{10} were co-expressed in *E. coli* BL21 (DE3)

(Novagen). Cells were lyzed by sonication in Buffer A, and the supernatant was applied to HisPur cobalt resin. The resin-bound protein was treated with Buffer A containing additional 0.1 mM phytate to remove the CPD-His_{10} tag, and the protein was eluted from the column with Buffer A. The sample was further purified with a HiTrap Q anion exchange column and HiLoad 26/60 Superdex 75 gel filtration column, equilibrated in Buffer A containing additional 1 mM DTT. The purified complex was concentrated to 20 mg ml^{-1} using Amicon Ultra 30K. SelMet-substituted $ScpA^{\Delta C}$–ScpB was produced in the *E. coli* B834 (DE3) strain, and purified as described above. Initial crystals of $ScpA^{\Delta C}$–ScpB grew in a solution containing 200 mM trimethylamine N-oxide, 20 % polyethylene glycol monomethyl ether 2,000 and 100 mM Tris-HCl (pH 8.5). Larger single crystals were obtained by microseeding at 22° C from the same precipitant solution. A SAD data set was collected with a crystal of the complex of SelMet-$ScpA^{\Delta C}$–ScpB at Beamline 5C at the Pohang Accelerator Laboratory, Korea. The selenium positions were identified by the program HySS[15] and used for phase determination by Phaser[16]. Subsequent density modification was performed using RESOLVE[17], manual model building using Coot[6] and the structure refinement using CNS[14]. The final model does not include residues 1-7, 76-78 and 156-160 of ScpA, residues 1 and 168-183 of $ScpB_A$ and residues 1 and 169-183 of $ScpB_B$.

Modeling of cross-linking kinetics

For modeling of cross-linking reactions, we made simplifying assumptions that

I) cross-linking at the binding interfaces does not perturb the binding equilibrium in the timescale of the experiment

II) complexes exist near compositional homogeneity, i.e. the population is dominated by a single architecture and less abundant forms can be neglected.

We then described cross-linking at a given binding interface by two competing irreversible reactions. One reaction results in the formation of a cysteine-BMOE-cysteine cross-link and proceeds with a rate constant k. The second reaction irreversibly inactivates the site by incorporating BMOE molecules at both cysteine residues (cysteine-BMOE and BMOE-cysteine) with a rate constant k_i. Rate constants for a given model were estimated by performing cross-linking at only one type of interface. These rate constants were then used to predict the outcome of a reaction in which both types of interfaces are cross-linked simultaneously.

For cross-linking at a single type of interface, rate equations and starting conditions for transformation of species A (non-cross-linked interface) into species X (cross-linked interface) or into species I (inhibited interface) are

a'[t] = -k a[t] - ki a[t]
i'[t] = ki a[t]
x'[t] = k a[t]
a[0] = 1
i[0] = 0
x[0] = 0

with a[t], i[t] and x[t] being concentrations of A, I or X at time t and a'[t], i'[t] and x'[t] being their time derivatives.

We assumed that inactivating reactions are equally fast at both types of interfaces, and solved rate equations numerically for k_i = 1 and different values of k between 0.01 and 10 using Wolfram Mathematica. Since *in vivo* BMOE cross-linking was fast and proceeded to completion, we generally used the relaxed system (t = 20) to compare theoretical concentrations with experimental data. To estimate k for cross-linking at neck or cap it was necessary to

transform concentrations reported by the kinetic model into fluorescence intensities observable after SDS-PAGE (**Fig. 4c**). Due to different occupancies of binding sites in models 1-4 (**Fig. 4b**), species A, I and X contribute differently to band intensities depending on the model:

Model 1 and 2 fluorescence intensities (full occupancy, single site cross-link)
Band I: a[20] + i[20]
Band II/III: x[20]

Model 3 and 4 fluorescence intensities (half occupancy, single site cross-link)
Band I: (2*a[20] + 2*i[20] + x[20])/2
Band II/III: x[20]/2

Single cross-linking at neck or cap interface, respectively, resulted in similar fluorescence intensities of product bands (30 ± 3 % and 31 ± 1 %, respectively). We therefore estimated rate constants for both reactions to be k = 1/2.35 (model 1 and 2) and k = 1.5 (model 3 and 4).
For each model, we then set up rate equations for simultaneous cross-linking at both interfaces. In these, each binding site reacts from the non-cross-linked state to a cross-linked or inhibited state. The model with four cross-bridged binding sites (model 1) led to 81 possible reaction intermediates/end products. Models with only two occupied binding sites (model 3 and 4) or two pairs of binding sites that can be regarded independently (model 2) led to 9 possible reaction intermediates/end products. Rate equations were then solved numerically with rate constants estimated from single site cross-linking. Finally, we transformed concentrations into predicted band intensities for comparison with experimental data (values reported in **Fig. 4c**). Full Mathematica code for double cross-link kinetic models and their transformation into predicted band intensities is given in Appendix I.

Purification and mass-spectrometric analysis of cross-linked prokaryotic condensin species from *Bacillus subtilis*

For purification of cross-linked Smc–ScpA species, Smc cysteine mutants were tagged with a C-terminal His_{12}-tag at the endogenous locus by double cross-over recombination. Cells were grown in LB and cross-linked with BMOE as described above, except that the buffer also contained a protease inhibitor cocktail (Sigma). Material from three independent cross-linking reactions was pooled and native protein extracts were prepared by freezing the 2-ME quenched cell suspension in liquid nitrogen, mechanical grinding in a swing mill, and 20 min centrifugation at 50,000 x g. The extract was adjusted to 1 M NaCl, 1 % Triton X-100 (TX-100) and 50 mM imidazole in PBS (final concentrations). Proteins were bound to MagneHis particles (Promega) in triplicates, washed extensively in PBS containing 1 M NaCl, 1 % TX-100, 50 mM imidazole (final concentrations) and eluted in PBS containing 1 M NaCl, 0.05 % TX-100, 500 mM imidazole. Proteins were precipitated by TCA–NaDOC, and an aliquot from each replicate was resolved by SDS-PAGE. Proteins were stained with Coomassie Blue and tryptic peptides were analyzed by LC–MS. For each replicate, only peptides were regarded that had been detected in all LC–MS runs. Single peptide intensities of Smc and ScpA derived from band IV and V (species with unknown stoichiometry) were separately plotted against peptide intensities from band II and III (species with 1:1 stoichiometry) for each replicate. One data-set for band III was omitted due to low signals and strong variance in Smc intensities. Data were line fitted and slopes obtained for Smc and ScpA peptides were put into relation. This resulted in five estimates for Smc–ScpA ratios in bands IV and V. Data are presented as geometric mean ± standard deviation.

In vitro cross-linking of DnaA

Oligomers of DnaA(N191C A198C L294R) were assembled and cross-linked in the presence of pUC18 and ATP exactly as described[1].

Analytical ultracentrifugation

Sedimentation velocity experiments were performed on an Optima XL-I analytical ultracentrifuge (Beckman Inc., Palo Alto, Ca, U.S.A.) using an An 60 Ti rotor and double-sector epon centerpieces. The proteins were prepared at 7.6 mg ml^{-1} (i.e. 130 μM) in 25 mM Tris-HCl pH 7.0, 200 mM NaCl. Buffer density and viscosity was measured using a DMA 5,000 densitometer and an AMVn viscosimeter, respectively (both Anton Paar, Graz, Austria). Protein concentration distribution was monitored at 280 nm, at 50,000 rpm and 20° C. Time-derivative analysis was computed using the SEDFIT software package, version 12.1b[18], resulting in a c(s) distribution and an estimate for the molecular weight Mf (from the sedimentation coefficient and the diffusion coefficient, as inferred from the broadening of the sedimentation boundary, assuming all observed species share the same frictional coefficient f/f_0) [18].

Appendix I - Mathematica code for kinetic models of cross-linking reactions

Model 1 - Smc_2-$ScpA_2$ (bridged)

```
(*Rate constants k1 and k1i: Neck interface
Rate constants k2 and k2i: Cap interface
*)
k1i = 1;
k2i = 1;
k1 = k1i/2.35;
k2 = k2i/2.35;

sol = NDSolve[{

      (*Nomenclature:
      a: non-cross-linked complex (= 2 Smc + 2 ScpA);
        w,x,y or z: complex cross-linked at site W (neck on head 1),
      X (neck on head 2), Y (cap on head 1) or Z (cap on head 2), respectively;
        iw,ix,iy or iz: complex inhibited at site W, X, Y, or Z, respectively;
        Higher order species are described by multiple letters,
      with cross-linked sites called first and inhibited sites following the letter i, e.g.
      species wyixz is cross-
      linked at W and Y and inhibited at X and Z
      *)

      (*Level 0*)
      a'[t] == -2*k1 a[t] - 2*k2 a[t] - 2*k1i a[t] - 2*k2i a[t],

      (*Level 1*)
      w'[t] == k1 a[t] - (2*k2 + 2*k2i + k1 + k1i) w[t],
      x'[t] == k1 a[t] - (2*k2 + 2*k2i + k1 + k1i) x[t],
      y'[t] == k2 a[t] - (2*k1 + 2*k1i + k2 + k2i) y[t],
      z'[t] == k2 a[t] - (2*k1 + 2*k1i + k2 + k2i) z[t],
      iw'[t] == k1i a[t] - (2*k2 + 2*k2i + k1 + k1i) iw[t],
      ix'[t] == k1i a[t] - (2*k2 + 2*k2i + k1 + k1i) ix[t],
      iy'[t] == k2i a[t] - (2*k1 + 2*k1i + k2 + k2i) iy[t],
      iz'[t] == k2i a[t] - (2*k1 + 2*k1i + k2 + k2i) iz[t],

      (*Level 2*)
      wx'[t] == k1 w[t] + k1 x[t] - (2*k2 + 2*k2i) wx[t],
      wy'[t] == k2 w[t] + k1 y[t] - (k1 + k2 + k1i + k2i) wy[t],
      wz'[t] == k2 w[t] + k1 z[t] - (k1 + k2 + k1i + k2i) wz[t],
      wix'[t] == k1i w[t] + k1 ix[t] - (2*k2 + 2*k2i) wix[t],
      wiy'[t] == k2i w[t] + k1 iy[t] - (k1 + k2 + k1i + k2i) wiy[t],
      wiz'[t] == k2i w[t] + k1 iz[t] - (k1 + k2 + k1i + k2i) wiz[t],
      xy'[t] == k2 x[t] + k1 y[t] - (k1 + k2 + k1i + k2i) xy[t],
      xz'[t] == k2 x[t] + k1 z[t] - (k1 + k2 + k1i + k2i) xz[t],
      xiw'[t] == k1i x[t] + k1 iw[t] - (2*k2 + 2*k2i) xiw[t],
      xiy'[t] == k2i x[t] + k1 iy[t] - (k1 + k2 + k1i + k2i) xiy[t],
      xiz'[t] == k2i x[t] + k1 iz[t] - (k1 + k2 + k1i + k2i) xiz[t],
      yz'[t] == k2 y[t] + k2 z[t] - (2*k1 + 2*k1i) yz[t],
      yiw'[t] == k1i y[t] + k2 iw[t] - (k1 + k2 + k1i + k2i) yiw[t],
      yix'[t] == k1i y[t] + k2 ix[t] - (k1 + k2 + k1i + k2i) yix[t],
      yiz'[t] == k2i y[t] + k2 iz[t] - (2*k1 + 2*k1i) yiz[t],
      ziw'[t] == k1i z[t] + k2 iw[t] - (k1 + k2 + k1i + k2i) ziw[t] ,
      zix'[t] == k1i z[t] + k2 ix[t] - (k1 + k2 + k1i + k2i) zix[t] ,
      ziy'[t] == k2i z[t] + k2 iy[t] - (2*k1 + 2*k1i) ziy[t],
      iwx'[t] == k1i iw[t] + k1i ix[t] - (2*k2 + 2*k2i) iwx[t],
      iwy'[t] == k2i iw[t] + k1i iy[t] - (k1 + k2 + k1i + k2i) iwy[t],
      iwz'[t] == k2i iw[t] + k1i iz[t] - (k1 + k2 + k1i + k2i) iwz[t],
      ixy'[t] == k2i ix[t] + k1i iy[t] - (k1 + k2 + k1i + k2i) ixy[t],
```

```
ixz'[t] == k2i ix[t] + k1i iz[t] - (k1 + k2 + k1i + k2i) ixz[t],
iyz'[t] == k2i iy[t] + k2i iz[t] - (2*k1 + 2*k1i) iyz[t],

(*Level 3*)
wxy'[t] == k2 wx[t] + k1 wy[t] + k1 xy[t] - (k2 + k2i) wxy[t],
wxz'[t] == k2 wx[t] + k1 wz[t] + k1 xz[t] - (k2 + k2i) wxz[t],
wxiy'[t] == k2i wx[t] + k1 wiy[t] + k1 xiy[t] - (k2 + k2i) wxiy[t],
wxiz'[t] == k2i wx[t] + k1 wiz[t] + k1 xiz[t] - (k2 + k2i) wxiz[t],
wyz'[t] == k2 wy[t] + k2 wz[t] + k1 yz[t] - (k1 + k1i) wyz[t],
wyix'[t] == k1i wy[t] + k2 wix[t] + k1 yix[t] - (k2 + k2i) wyix[t],
wyiz'[t] == k2i wy[t] + k2 wiz[t] + k1 yiz[t] - (k1 + k1i) wyiz[t],
wzix'[t] == k1i wz[t] + k2 wix[t] + k1 zix[t] - (k2 + k2i) wzix[t],
wziy'[t] == k2i wz[t] + k2 wiy[t] + k1 ziy[t] - (k1 + k1i) wziy[t],
xyz'[t] == k2 xy[t] + k2 xz[t] + k1 yz[t] - (k1 + k1i) xyz[t],
xyiw'[t] == k1i xy[t] + k2 xiw[t] + k1 yiw[t] - (k2 + k2i) xyiw[t],
xyiz'[t] == k2i xy[t] + k2 xiz[t] + k1 yiz[t] - (k1 + k1i) xyiz[t],
xziw'[t] == k1i xz[t] + k2 xiw[t] + k1 ziw[t] - (k2 + k2i) xziw[t],
xziy'[t] == k2i xz[t] + k2 xiy[t] + k1 ziy[t] - (k1 + k1i) xziy[t],
yziw'[t] == k1i yz[t] + k2 yiw[t] + k2 ziw[t] - (k1 + k1i) yziw[t],
yzix'[t] == k1i yz[t] + k2 yix[t] + k2 zix[t] - (k1 + k1i) yzix[t],
wixy'[t] ==
  k2i wix[t] + k1i wiy[t] + k1 ixy[t] - (k2 + k2i) wixy[t],
wixz'[t] ==
  k2i wix[t] + k1i wiz[t] + k1 ixz[t] - (k2 + k2i) wixz[t],
wiyz'[t] ==
  k2i wiy[t] + k2i wiz[t] + k1 iyz[t] - (k1 + k1i) wiyz[t],
xiwy'[t] ==
  k2i xiw[t] + k1i xiy[t] + k1 iwy[t] - (k2 + k2i) xiwy[t],
xiwz'[t] ==
  k2i xiw[t] + k1i xiz[t] + k1 iwz[t] - (k2 + k2i) xiwz[t],
xiyz'[t] ==
  k2i xiy[t] + k2i xiz[t] + k1 iyz[t] - (k1 + k1i) xiyz[t],
yiwx'[t] ==
  k1i yiw[t] + k1i yix[t] + k2 iwx[t] - (k2 + k2i) yiwx[t],
yiwz'[t] ==
  k2i yiw[t] + k1i yiz[t] + k2 iwz[t] - (k1 + k1i) yiwz[t],
yixz'[t] ==
  k2i yix[t] + k1i yiz[t] + k2 ixz[t] - (k1 + k1i) yixz[t],
ziwx'[t] ==
  k1i ziw[t] + k1i zix[t] + k2 iwx[t] - (k2 + k2i) ziwx[t],
ziwy'[t] ==
  k2i ziw[t] + k1i ziy[t] + k2 iwy[t] - (k1 + k1i) ziwy[t],
zixy'[t] ==
  k2i zix[t] + k1i ziy[t] + k2 ixy[t] - (k1 + k1i) zixy[t],
iwxy'[t] ==
  k2i iwx[t] + k1i iwy[t] + k1i ixy[t] - (k2 + k2i) iwxy[t],
iwxz'[t] ==
  k2i iwx[t] + k1i iwz[t] + k1i ixz[t] - (k2 + k2i) iwxz[t],
iwyz'[t] ==
  k2i iwy[t] + k2i iwz[t] + k1i iyz[t] - (k1 + k1i) iwyz[t],
ixyz'[t] ==
  k2i ixy[t] + k2i ixz[t] + k1i iyz[t] - (k1 + k1i) ixyz[t],

(*Level 4*)
wxyz'[t] == k2 wxy[t] + k2 wxz[t] + k1 wyz[t] + k1 xyz[t],
wxyiz'[t] == k2i wxy[t] + k2 wxiz[t] + k1 wyiz[t] + k1 xyiz[t],
wxziy'[t] == k2i wxz[t] + k2 wxiy[t] + k1 wziy[t] + k1 xziy[t],
wyzix'[t] == k1i wyz[t] + k2 wyix[t] + k2 wzix[t] + k1 yzix[t],
xyziw'[t] == k1i xyz[t] + k2 xyiw[t] + k2 xziw[t] + k1 yziw[t],
wxiyz'[t] == k2i wxiy[t] + k2i wxiz[t] + k1 wiyz[t] + k1 xiyz[t],
wyixz'[t] == k2i wyix[t] + k1i wyiz[t] + k2 wixz[t] + k1 yixz[t],
wzixy'[t] == k2i wzix[t] + k1i wziy[t] + k2 wixy[t] + k1 zixy[t],
```

```
xyiwz'[t] == k2i xyiw[t] + k1i xyiz[t] + k2 xiwz[t] + k1 yiwz[t],
xziwy'[t] == k2i xziw[t] + k1i xziy[t] + k2 xiwy[t] + k1 ziwy[t],
yziwx'[t] == k1i yziw[t] + k1i yzix[t] + k2 yiwx[t] + k2 ziwx[t],
wixyz'[t] == k2i wixy[t] + k2i wixz[t] + k1i wiyz[t] + k1 ixyz[t],
xiwyz'[t] == k2i xiwy[t] + k2i xiwz[t] + k1i xiyz[t] + k1 iwyz[t],
yiwxz'[t] == k2i yiwx[t] + k1i yiwz[t] + k1i yixz[t] + k2 iwxz[t],
ziwxy'[t] == k2i ziwx[t] + k1i ziwy[t] + k1i zixy[t] + k2 iwxy[t],
iwxyz'[t] == k2i iwxy[t] + k2i iwxz[t] + k1i iwyz[t] + k1i ixyz[t],


(*Starting conditions*)
a[0] == 1,
w[0] == 0,
x[0] == 0,
y[0] == 0,
z[0] == 0,
iw[0] == 0,
ix[0] == 0,
iy[0] == 0,
iz[0] == 0,
wx[0] == 0,
wy[0] == 0,
wz[0] == 0,
wix[0] == 0,
wiy[0] == 0,
wiz[0] == 0,
xy[0] == 0,
xz[0] == 0,
xiw[0] == 0,
xiy[0] == 0,
xiz[0] == 0,
yz[0] == 0,
yiw[0] == 0,
yix[0] == 0,
yiz[0] == 0,
ziw[0] == 0,
zix[0] == 0,
ziy[0] == 0,
iwx[0] == 0,
iwy[0] == 0,
iwz[0] == 0,
ixy[0] == 0,
ixz[0] == 0,
iyz[0] == 0,
wxy[0] == 0,
wxz[0] == 0,
wxiy[0] == 0,
wxiz[0] == 0,
wyz[0] == 0,
wyix[0] == 0,
wyiz[0] == 0,
wzix[0] == 0,
wziy[0] == 0,
xyz[0] == 0,
xyiw[0] == 0,
xyiz[0] == 0,
xziw[0] == 0,
xziy[0] == 0,
yziw[0] == 0,
yzix[0] == 0,
wixy[0] == 0,
wixz[0] == 0,
```

```
      wiyz[0] == 0,
      xiwy[0] == 0,
      xiwz[0] == 0,
      xiyz[0] == 0,
      yiwx[0] == 0,
      yiwz[0] == 0,
      yixz[0] == 0,
      ziwx[0] == 0,
      ziwy[0] == 0,
      zixy[0] == 0,
      iwxy[0] == 0,
      iwxz[0] == 0,
      iwyz[0] == 0,
      ixyz[0] == 0,
      wxyz[0] == 0,
      wxyiz[0] == 0,
      wxziy[0] == 0,
      wyzix[0] == 0,
      xyziw[0] == 0,
      wxiyz[0] == 0,
      wyixz[0] == 0,
      wzixy[0] == 0,
      xyiwz[0] == 0,
      xziwy[0] == 0,
      yziwx[0] == 0,
      wixyz[0] == 0,
      xiwyz[0] == 0,
      yiwxz[0] == 0,
      ziwxy[0] == 0,
      iwxyz[0] == 0
      },
     {a, w, x, y, z, iw, ix, iy, iz, wx, wy, wz, wix, wiy, wiz, xy, xz,
      xiw, xiy, xiz, yz, yiw, yix, yiz, ziw, zix, ziy, iwx, iwy, iwz,
      ixy, ixz, iyz, wxy, wxz, wxiy, wxiz, wyz, wyix, wyiz, wzix, wziy,
      xyz, xyiw, xyiz, xziw, xziy, yziw, yzix, wixy, wixz, wiyz, xiwy,
      xiwz, xiyz, yiwx, yiwz, yixz, ziwx, ziwy, zixy, iwxy, iwxz, iwyz,
      ixyz, wxyz, wxyiz, wxziy, wyzix, xyziw, wxiyz, wyixz, wzixy,
      xyiwz, xziwy, yziwx, wixyz, xiwyz, yiwxz, ziwxy, iwxyz},
     {t, 0, 20}];


(*Plot to check if the system is relaxed at t = 20*)
Plot[Evaluate[{a[t], w[t], x[t], y[t], z[t], iw[t], ix[t], iy[t],
       iz[t], wx[t], wy[t], wz[t], wix[t], wiy[t], wiz[t], xy[t], xz[t],
       xiw[t], xiy[t], xiz[t], yz[t], yiw[t], yix[t], yiz[t], ziw[t],
       zix[t], ziy[t], iwx[t], iwy[t], iwz[t], ixy[t], ixz[t], iyz[t],
       wxy[t], wxz[t], wxiy[t], wxiz[t], wyz[t], wyix[t], wyiz[t],
       wzix[t], wziy[t], xyz[t], xyiw[t], xyiz[t], xziw[t], xziy[t],
       yziw[t], yzix[t], wixy[t], wixz[t], wiyz[t], xiwy[t], xiwz[t],
       xiyz[t], yiwx[t], yiwz[t], yixz[t], ziwx[t], ziwy[t], zixy[t],
       iwxy[t], iwxz[t], iwyz[t], ixyz[t], wxyz[t], wxyiz[t], wxziy[t],
       wyzix[t], xyziw[t], wxiyz[t], wyixz[t], wzixy[t], xyiwz[t],
       xziwy[t], yziwx[t], wixyz[t], xiwyz[t], yiwxz[t], ziwxy[t],
       iwxyz[t]} /. sol], {t, 0, 20}, PlotRange -> {Full, {0, 1}}]

(*Model 1 predictions: Only single cross-links contribute to bands II
and III, all other species are summed into band V*)
model1bandsend = {
    {{}, "Model 1 band intensities"},
    {"Band I",
     Evaluate[(wyixz[20] + xziwy[20] + wixyz[20] + xiwyz[20] +
           yiwxz[20] + ziwxy[20] + 2*iwxyz[20])/2 /. sol]},
```

```
    {"Band II",
      Evaluate[(2*wxiyz[20] + wixyz[20] + xiwyz[20])/2 /. sol]},
    {"Band III",
      Evaluate[(2*yziwx[20] + yiwxz[20] + ziwxy[20])/2 /. sol]},
    {"Band V",
      Evaluate[(2*wxyz[20] + 2*wxyiz[20] + 2*wxziy[20] + 2*wyzix[20] +
            2*xyziw[20] + 2*wzixy[20] + 2*xyiwz[20] + wyixz[20] +
            xziwy[20])/2 /. sol]}
    };

(*Intensity prediction table*)
TableForm[model1bandsend]
```

Model 2 - Smc_2ScpA_2 (not bridged)

```
(*Rate constants k1 and k1i: Neck interface
Rate constants k2 and k2i: Cap interface
*)
k1i = 1;
k2i = 1;
k1 = k1i/2.35;
k2 = k1i/2.35;

(*Nomenclature:
a: non-cross-linked complex (= 1 Smc + 1 ScpA);
  x: complex cross-linked at neck;
  y: complex cross-linked at cap;
  i1: complex inhibited at neck;
  i2: complex inhibited at cap;
  i3: complex inhibited at both sites;
*)
sol = NDSolve[{
      a'[t] == -k1 a[t] - k2 a[t] - k1i a[t] - k2i a[t],
      i1'[t] == k1i a[t] - k2i i1[t] - k2 i1[t],
      i2'[t] == k2i a[t] - k1i i2[t] - k1 i2[t],
      i3'[t] == k2i i1[t] + k1i i2[t],
      x'[t] == k1 a[t] - k2 x[t] - k2i x[t],
      y'[t] == k2 a[t] - k1 y[t] - k1i y[t],
      xi'[t] == k2i x[t] + k1 i2[t],
      yi'[t] == k1i y[t] + k2 i1[t],
      b'[t] == k2 x[t] + k1 y[t],
      a[0] == 1,
      i1[0] == 0,
      i2[0] == 0,
      i3[0] == 0,
      x[0] == 0,
      y[0] == 0,
      xi[0] == 0,
      yi[0] == 0,
      b[0] == 0
      },
    {a, i1, i2, i3, x, y, xi, yi, b},
    {t, 0, 20}];

(*Plot to check if the system is relaxed at t = 20*)
model2plot = Plot[Evaluate[{
       a[t], i1[t], i2[t], i3[t], x[t], y[t], xi[t], yi[t], b[t]
       } /. sol], {t, 0, 20}, PlotRange -> {Full, {0, 1}}]

(*Intensity predictions*)
```

```
model2bandsend = {
    {{}, "Model 2 band intensities"},
    {"Band I", Evaluate[(a[20] + i3[20] + i1[20] + i2[20]) /. sol]},
    {"Band II", Evaluate[(x[20] + xi[20]) /. sol]},
    {"Band III", Evaluate[(y[20] + yi[20]) /. sol]},
    {"Band V", Evaluate[(b[20]) /. sol]}
    };

TableForm[model2bandsend]
```

Model 3 - Smc_2-ScpA (not bridged)

```
(*Rate constants k1 and k1i: Neck interface
Rate constants k2 and k2i: Cap interface
*)
k1i = 1;
k2i = 1;
k1 = k1i*1.5;
k2 = k1i*1.5;

(*Nomenclature:
a: non-cross-linked complex (= 2 Smc + 1 ScpA);
  x: complex cross-linked at neck;
  y: complex cross-linked at cap;
  i1: complex inhibited at neck;
  i2: complex inhibited at cap;
  i3: complex inhibited at both sites;
*)
sol = NDSolve[{
       a'[t] == -k1 a[t] - k2 a[t] - k1i a[t] - k2i a[t],
       i1'[t] == k1i a[t] - k2i i1[t] - k2 i1[t],
       i2'[t] == k2i a[t] - k1i i2[t] - k1 i2[t],
       i3'[t] == k2i i1[t] + k1i i2[t],
       x'[t] == k1 a[t] - k2 x[t] - k2i x[t],
       y'[t] == k2 a[t] - k1 y[t] - k1i y[t],
       xi'[t] == k2i x[t] + k1 i2[t],
       yi'[t] == k1i y[t] + k2 i1[t],
       b'[t] == k2 x[t] + k1 y[t],
       a[0] == 1,
       i1[0] == 0,
       i2[0] == 0,
       i3[0] == 0,
       x[0] == 0,
       y[0] == 0,
       xi[0] == 0,
       yi[0] == 0,
       b[0] == 0
       },
     {a, i1, i2, i3, x, y, xi, yi, b},
     {t, 0, 20}];

(*Plot to check if the system is relaxed at t = 20*)
model3plot = Plot[Evaluate[{
        a[t], i1[t], i2[t], i3[t], x[t], y[t], xi[t], yi[t], b[t]
        } /. sol], {t, 0, 20}, PlotRange -> {Full, {0, 1}}]

(*Intensity predictions*)
model3bandsend = {
    {{}, "Model 3 band intensities"},
    {"Band I",
```

```
    Evaluate[(2*a[20] + 2*i3[20] + 2*i1[20] + 2*i2[20] + x[20] +
          xi[20] + y[20] + yi[20] + b[20])/2 /. sol]},
   {"Band II", Evaluate[(x[20] + xi[20])/2 /. sol]},
   {"Band III", Evaluate[(y[20] + yi[20])/2 /. sol]},
   {"Band V", Evaluate[(b[20])/2 /. sol]}
   };

TableForm[model3bandsend]
```

Model 4 - Smc_2-ScpA (bridged)

```
(*Rate constants k1 and k1i: Neck interface
Rate constants k2 and k2i: Cap interface
*)
k1i = 1;
k2i = 1;
k1 = k1i*1.5;
k2 = k1i*1.5;

(*Nomenclature:
a: non-cross-linked complex (= 2 Smc + 1 ScpA);
  x: complex cross-linked at neck;
  y: complex cross-linked at cap;
  i1: complex inhibited at neck;
  i2: complex inhibited at cap;
  i3: complex inhibited at both sites;
*)
sol = NDSolve[{
     a'[t] == -k1 a[t] - k2 a[t] - k1i a[t] - k2i a[t],
     i1'[t] == k1i a[t] - k2i i1[t] - k2 i1[t],
     i2'[t] == k2i a[t] - k1i i2[t] - k1 i2[t],
     i3'[t] == k2i i1[t] + k1i i2[t],
     x'[t] == k1 a[t] - k2 x[t] - k2i x[t],
     y'[t] == k2 a[t] - k1 y[t] - k1i y[t],
     xi'[t] == k2i x[t] + k1 i2[t],
     yi'[t] == k1i y[t] + k2 i1[t],
     b'[t] == k2 x[t] + k1 y[t],
     a[0] == 1,
     i1[0] == 0,
     i2[0] == 0,
     i3[0] == 0,
     x[0] == 0,
     y[0] == 0,
     xi[0] == 0,
     yi[0] == 0,
     b[0] == 0
     },
    {a, i1, i2, i3, x, y, xi, yi, b},
    {t, 0, 20}];

(*Plot to check if the system is relaxed at t = 20*)
model4plot = Plot[Evaluate[{
      a[t], i1[t], i2[t], i3[t], x[t], y[t], xi[t], yi[t], b[t]
      } /. sol], {t, 0, 20}, PlotRange -> {Full, {0, 1}}]

(*Intensity predictions*)
model4bandsend = {
   {{}, "Model 4 band intensities"},
   {"Band I",
     Evaluate[(2*a[20] + 2*i3[20] + 2*i1[20] + 2*i2[20] + x[20] +
```

```
        xi[20] + y[20] + yi[20])/2 /. sol]},
    {"Band II", Evaluate[(x[20] + xi[20])/2 /. sol]},
    {"Band III", Evaluate[(y[20] + yi[20])/2 /. sol]},
    {"Band V", Evaluate[(2*b[20])/2 /. sol]}
    };

TableForm[model4bandsend]
```

References

1. Scholefield, G., Errington, J. & Murray, H. Soj/ParA stalls DNA replication by inhibiting helix formation of the initiator protein DnaA. *EMBO J* **31**, 1542-55 (2012).
2. Dominguez-Cuevas, P., Mercier, R., Leaver, M., Kawai, Y. & Errington, J. The rod to L-form transition of Bacillus subtilis is limited by a requirement for the protoplast to escape from the cell wall sacculus. *Mol Microbiol* **83**, 52-66 (2012).
3. Studier, F.W. Protein production by auto-induction in high density shaking cultures. *Protein Expr Purif* **41**, 207-34 (2005).
4. Kabsch, W. Automatic Processing of Rotation Diffraction Data from Crystals of Initially Unknown Symmetry and Cell Constants. *J Appl Crystallogr* **26**, 795-800 (1993).
5. Cowtan, K. The Buccaneer software for automated model building. 1. Tracing protein chains. *Acta Crystallogr D Biol Crystallogr* **62**, 1002-11 (2006).
6. Emsley, P. & Cowtan, K. Coot: model-building tools for molecular graphics. *Acta Crystallogr D Biol Crystallogr* **60**, 2126-32 (2004).
7. Adams, P.D. et al. PHENIX: a comprehensive Python-based system for macromolecular structure solution. *Acta Crystallogr D Biol Crystallogr* **66**, 213-21 (2010).
8. Lammens, A., Schele, A. & Hopfner, K.P. Structural biochemistry of ATP-driven dimerization and DNA-stimulated activation of SMC ATPases. *Curr Biol* **14**, 1778-82 (2004).
9. Shen, A. et al. Simplified, Enhanced Protein Purification Using an Inducible, Autoprocessing Enzyme Tag. *PLoS ONE* **4**, e8119 (2009).
10. Schneider, T.R. & Sheldrick, G.M. Substructure solution with SHELXD. *Acta Crystallographica Section D* **58**, 1772-1779 (2002).
11. De La Fortelle, E. & Bricogne, G. Maximum-likelihood heavy-atom parameter refinement for multiple isomorphous replacement and multiwavelength anomalous diffraction methods. *Macromolecular Crystallography, Pt A* **276**, 472-494 (1997).
12. Abrahams, J.P. & Leslie, A.G. Methods used in the structure determination of bovine mitochondrial F1 ATPase. *Acta Crystallogr D Biol Crystallogr* **52**, 30-42 (1996).
13. Perrakis, A., Morris, R. & Lamzin, V.S. Automated protein model building combined with iterative structure refinement. *Nat Struct Mol Biol* **6**, 458-463 (1999).
14. Brunger, A.T. et al. Crystallography & NMR system: A new software suite for macromolecular structure determination. *Acta Crystallogr D Biol Crystallogr* **54**, 905-21 (1998).
15. Grosse-Kunstleve, R.W. & Adams, P.D. Substructure search procedures for macromolecular structures. *Acta Crystallogr D Biol Crystallogr* **59**, 1966-73 (2003).
16. McCoy, A.J. et al. Phaser crystallographic software. *J Appl Crystallogr* **40**, 658-674 (2007).
17. Terwilliger, T.C. Statistical density modification with non-crystallographic symmetry. *Acta Crystallogr D Biol Crystallogr* **58**, 2082-6 (2002).
18. Schuck, P. Size-distribution analysis of macromolecules by sedimentation velocity ultracentrifugation and lamm equation modeling. *Biophys J* **78**, 1606-19 (2000).